REVISION 2 ms #4238

Clay minerals thermometry: A comparative study based on high-spatial-resolution analyses of illite and chlorite in Gulf Coast sandstones (Texas, USA)

Franck Bourdelle[1,2,3,*], Teddy Parra[2], Olivier Beyssac[1], Christian Chopin[3,†], and Olivier Vidal[4]

[1] IMPMC, UPMC-CNRS, Campus Jussieu, Case courrier 115, 4 place Jussieu, 75005 Paris, France.

[2] IFP Energies nouvelles, 1 et 4 avenue de Bois Préau, 92852 Rueil-Malmaison cedex, France.

[3] Laboratoire de Géologie, Ecole normale supérieure - CNRS, 24 rue Lhomond, 75231 Paris cedex 5, France.

[4] CNRS, Université Joseph Fourier Grenoble, ISTerre, BP 53, 1381 rue de la piscine, 38041 Grenoble Cedex, France.

* E-mail address: franck.bourdelle@gmail.com

† E-mail address: christian.chopin@ens.fr

Abstract

A high-resolution analytical technique combining Focused Ion Beam (FIB) milling and Analytical Electron Microscopy (AEM) analysis has been applied to a series of sandstone core samples from the Gulf Coast (Texas, USA). The nanoscale compositional variations of K-deficient mica and chlorite flakes show that rim compositions are the most likely to

approach equilibrium compositions, whereas core compositions may be relict, especially for illite-like phases. These rim analyses were used to test existing empirical or thermodynamically formulated thermo(baro)meters against maximum temperatures, which are perfectly constrained for the selected samples as they were measured *in situ* during drilling (100-230°C and 300-1200 bars). The results show that most of the empirical models overestimate the temperature, while thermodynamic models yields reasonable estimates for diagenetic to anchizonal conditions, especially if the Fe^{3+} content is taken into account. This study clearly shows that phyllosilicates thermometry is reliable when combined with an analytical technique giving access to the fine-scale compositional variations that may represent local equilibration, whereas using micrometric compositional analysis precludes trustworthy application of such thermometers.

Key-words: illite, chlorite, zonation, thermometry, diagenesis, Gulf Coast.

Introduction

Phyllosilicates are widespread minerals in most diagenetic and low-grade metamorphic rocks. For a long time, their compositional variations have attracted interest as potential markers of diagenesis and burial conditions like temperature (*T*), pressure (*P*), rock composition, or fluid availability (e.g. Walshe 1986; Vidal and Parra 2000). These compositional variations reflect the wide possible range of a number of substitutions in phyllosilicates, e.g. di-tri-octahedral, Tschermak or Fe–Mg exchange. Establishing a quantitative link between composition and formation conditions has therefore been a long pursued goal, with two main approaches: empirical calibrations and thermodynamic modelling.

In the empirical case, Cathelineau and Nieva (1985) and Cathelineau (1988) established a correlation between chlorite tetrahedral Al occupancy (noted ^{IV}Al) and temperature. Their empirical calibrations were subsequently refined by Kranidiotis and McLean (1987), Jowett (1991), Zang and Fyfe (1995) and Xie et al. (1997) to account for the chlorite Mg and Fe contents, which depend primarily on the bulk-rock composition. These empirical thermometers can be easily implemented, but they provide contrasted, sometimes unrealistic, temperature estimates (e.g. De Caritat et al 1993; Essene and Peacor 1995; Vidal et al 1999; Parra et al 2001). More robust thermodynamic solutions have been proposed (Helgeson et al 1978; Helgeson and Aagaard, 1985; Walshe 1986; Aagard and Jahren 1992; Hutcheon 1990; Vidal and Parra 2000; Vidal et al. 2001, 2005, 2006; Parra et al. 2002; Inoue et al. 2009; Dubacq et al. 2010), but they require knowledge of the thermodynamic properties for numerous end-members as well as solid-solution mixing parameters.

The aim of the present study is to compare the results of such thermometers when applied to a low-temperature, diagenetic sample series of well cores for which a direct, *in situ* physical measure of temperature and pressure is available. Indeed, most chlorite and illite thermometers were calibrated either in specific conditions, e.g. a hydrothermal system for Cathelineau and Nieva (1985) study, or at relatively high temperatures that were indirectly derived from petrological data, like phase-equilibria, fluid-inclusion or vitrinite-reflectance thermometry.

In addition, several generations of clay minerals showing various compositions generally coexist in the same rock sample, from detrital to authigenic to metamorphic, either as discrete crystals in distinct sites, or as zoned crystals with successive overgrowths on relict cores, which may record part of the clay history. In order to be able to decipher this record in spite of the small grain sizes and expectedly fine scale of the chemical features, a high spatial analytical resolution is needed. The present study takes advantage of recent developments in

combining Focused Ion Beam (FIB) sectioning (e.g. Wirth 2004) and high-resolution transmission electron microscopy (TEM) with coupled energy-dispersive X-ray analysis (EDX). This combination allows both a nanometre-scale resolution of chemical variations and then a detailed investigation of the compositional (and crystallization temperature) evolution of phyllosilicates in 2D at the thin-section scale, as it is classically made for metamorphic rocks with electron microprobe analysis (EMPA). The coupled FIB, TEM and EDX techniques were used to explore intracrystalline compositional variations, in an attempt at identifying the compositional domains that may record equilibration at peak temperatures for the key assemblages chlorite + quartz, chlorite + illite and illite + quartz. The relevant compositions were used to test empirical thermometers and the models proposed by Walshe (1986), Vidal et al. (2005) rearranged by Vidal et al. (2006), Inoue et al. (2009) and Dubacq et al. (2010) against the measured *T* and *P* in Gulf Coast drill-core samples, considering also the possible effect of the Fe^{3+}/Fe^{2+} ratio.

Samples and geological settings

Samples

Thirteen samples from 9 wells were taken from conventional drill cores of the Gulf Coast area (southern Texas, USA), available at the core repository, Bureau of Economic Geology and at University of Texas at Austin (USA). They were selected on the basis of their mineral contents (presence of chlorite, illite-chlorite contacts with a grain size allowing FIB cutting), and to cover the largest range of depth and temperature conditions as possible (cf. Appendix 1).

The selected samples are sandstones and shales of relatively uniform mineralogy, except for the relative amount of clays and/or carbonate cement (cf. Appendix 1). Samples

with low or preferably no carbonate content were chosen, to minimize modification of the activity of H_2O. These samples consist mostly of quartz (> 80%), with detrital feldspars, clays (detrital and authigenic) and a minor amount of carbonates (calcite and dolomite), organic matter and pyrite. Clay minerals refer to smectite, I/S, illite, chlorite and kaolinite. The analysed chlorites are devoid of 7 Å phases, as shown by TEM.

Pressure and temperature conditions: thermal history of the Gulf Coast

The last major tectonic event in the Gulf Coast area was the Triassic-Early Jurassic opening of the Gulf of Mexico. Then, the southern Texas remained tectonically quiet throughout the Cenozoic Era (Stanley 1986; Posey 1986), with a continuous marine deposition offshore. Thus, the temperature distribution within the sediments remained similar to the classic *T*-depth burial distribution during the Cenozoic, after the thermal anomaly resulting from rifting was dissipated (Nunn 1984). The selected samples are from onshore area, resulting of recent marine regression. At depth, some thermal anomalies exist locally due to advecting fluids moving along the growth faults (Jones 1975; Bodner and Sharp 1988). These anomalies might be due to the presence of salt beds at depth inducing heterogeneities in thermal conductivity (Bodner 1985), and from a thermal anomaly of the lithosphere (Bodner 1985). However, these thermal anomalies do not affect significantly the eastern area (Frio/Vicksburg fault zone; Pfeiffer 1989). As a consequence, we assume that the present-day *P*-*T* conditions are the maximum temperatures and maximum pressures reached by each of the samples since its deposition. This assumption was made previously by several equivalent studies (e.g. Hillier and Velde, 1991) and is supported by (i) the regular subsidence and a continuous sediment deposition (Royden et al 1980) during the Cretaceous and the Cenozoic and (ii) the low erosion rates, from which one can induce that sedimentary deposits are likely to be near their maximum burial depth now (Dutton and Loucks 2010).

Temperature and pressure constraints are bottom hole *T* and *P* (noted BHT and BHP, respectively), which were collected from oil and gas well-log headers (purchase by the Bureau of Economic Geology), or from literature recapitulating well-log information (Bodner 1985; Loucks et al 1979; Pfeiffer 1989; McKenna 1997; Bebout et al 1982; Kosters et al 1989; Dodge and Posey 1981; Lynch 1994). The BHT were corrected by the empirical method of Kehle (1971), which was shown to approach the real temperature by 10 °C (Lynch, 1994). The BHP were also corrected, taking into account the drilling-mud density and the transition between hydropressure and geopressure regimes as determined by resistivity logs and porosity studies. Finally, the measured temperatures for the selected samples range from 100 to 230°C and the pressures range from 0.3 to 1.2 kbar (cf. Appendix 1). Theses results are considered as the maximum temperature or pressure undergone by the samples with a tentative uncertainty of ±20 °C (twice Kehle's method uncertainty) and ±100 bars (equivalent to ±700 m in depth).

Analytical procedure

A Scanning Electron Microprobe (SEM) study was carried out for precisely locating the clay minerals before FIB milling on the Hitachi S-2500 instrument at ENS, Paris, operated at 15 kV with a 1.5 nA current intensity. We then used a FIB 200 FEI of CP2M (University of Aix-Marseille), with a voltage of 30 kV, and a gallium beam. The cutting intensity varied from 5000 to 50 pA and we followed the protocol for FIB-section preparation given by Heaney et al. (2001). Samples were finally analyzed with a TEM-EDX/FIB coupled method and quantitative analyses were deduced and corrected thanks to the *t-O-protocol* (Van Cappellen and Doukhan 1994; Bourdelle et al. 2012). Twenty-three FIB thin sections were cut from 12 samples, across illite-chlorite contacts near one end of the interface, where

recrystallisation is the most likely. The thin foils were cut out with a size of approximately 15 µm by 5 µm and a thickness between 50 and 300 nm. To check for the preservation of the minerals crystalline structure after FIB-milling, lattice-fringe imaging was then systematically carried out with the TEM.

The FIB sections were analyzed with a TEM-EDX JEOL 2100-F at the Physics and Microanalysis Department of IFPEN (France), using a 200 kV voltage, a counting time of 60 s and a dead time lower than 15%. The current density was maintained at 1.3 pA/cm^{-2}. The sample tilt angle was 7°. In these conditions, the spot size was around 1 nm and defocused to 50 nm. The EDX analyzer was calibrated on paragonite (Na, Al), pyrophyllite (Al), talc (Mg), muscovite (Fe, Al, K), chlorite (Fe, Al), clintonite (Mg, Ca, Al) and phengite (Mg, Fe, K, Al) and the standardizations were checked against EMP analysis of reference clays (SMB-18; Kohler et al. 2009). Given the high spatial resolution, the analysis points were targeted to reveal within-grain compositional variations (Fig. 1) and, in the case of coexisting chlorite and mica, so as to obtain couples of analyses that may record local equilibrium under changing *P*-*T* conditions.

The structural formulae were calculated on the basis of 11 and 14 oxygens for illite-like phases and chlorites, respectively, with K, Na and Ca assigned to the interlayer. Several numerical criteria were applied to exclude poor-quality and/or contaminated analyses. For illite-like phases, analyses with either K + Na + Ca > 1 apfu, Si < 3 apfu or Si > 4 apfu were excluded. For chlorites, analyses with $K_2O + Na_2O + CaO > 1$ wt% (of the 100 wt% total of TEM-EDX analyses) were excluded.

Intracrystalline chemical variations: interpretation and implication for thermobarometry

From the high-spatial resolution dataset yielded by the analytical protocol, analyses were separated into two categories: crystal rim analyses performed at 50 nm of illite-chlorite contacts, and crystal-core analyses (Fig. 1). The comparison of core and rim analyses of illite and chlorite in the selected Gulf Coast samples reveals some systematic trends as a function of measured temperature (i.e. BHT). All the analyses obtained for 2:1 phyllosilicates show K as the dominant interlayer cation, with only traces of Na and Ca. From these observations, Figure 2 presents the K contents of 2:1 phyllosilicates *vs* measured temperature. In the grain cores of each sample, the K content ranges between ~0.5 and 0.8 to 0.98 apfu regardless of the temperature attained (examples of illite rims analyses in Table 1; cf. Appendix 2). In contrast, the maximum K content of the rim analyses increases from ~0.4-0.5 apfu (at ~100 °C) to 0.7-0.9 apfu (at ~230 °C), which reflects the compositional evolution due to illitization (e.g. Perry and Hower 1970; Cathelineau and Nieva 1985; Mathieu and Velde 1989; Lanson and Besson 1992; Battaglia 2004). The rim compositions with maximum K were thus considered to be the compositions closest to equilibrium compositions. Conversely, the K-rich core analyses obtained in the low-*T* samples most likely reflect inherited compositions of detrital material and were not considered further for thermometry. In contrast to the temperature-dependence of the K content, ^{VI}Al (between 1.5 and 2 apfu), Fe + Mg (about 0.6 apfu) contents and XFe (0.5 ± 0.1) show no evolution with temperature for the rim compositions. A variation with *T* of Si content is observable, but not obvious to decipher. The observed trend in K content (Fig. 2) and the possible trend in Si (or ^{IV}Al) content with temperature are accounted for by the combination of the pyrophyllitic (^{IV}Si $^{XII}\square$ = ^{IV}Al ^{XII}K) and Tschermak substitutions (^{IV}Si ^{VI}(Fe, Mg) = ^{IV}Al ^{VI}Al), or any linear combination of them like ^{VI}Al $^{XII}\square$ = ^{VI}Fe ^{XII}K (i.e. octahedral-interlayer exchange), where IV, VI and XII identify tetrahedral, octahedral and interlayer sites respectively, and $\square$ represents octahedral vacancies. According to the observed K contents, we are dealing with illite or K-smectite,

simply referred to as illite or K-deficient mica in the following since the thermometers tested consider them collectively.

The tetrahedral Al content (^{IV}Al) of core and rim chlorite grains shows a rough increase with *T*, as expected from earlier studies (Fig. 3). More surprising is the consistently (except at 129 and 191 °C) higher ^{IV}Al maximum value in core than in rim, which is opposite to the trend documented by e.g. Jahren (1991, in zoned authigenic chlorite crystals of the North Sea). This feature suggests that some crystal cores may be of dedrital origin and have retained the high ^{IV}Al content typical for metamorphic chlorites, with their inherent variability. For this reason, only the rim compositions of chlorite were considered for thermometry (examples of chlorite rims analyses are given Table 2 and Appendix 3). In details, these rim compositions of the Gulf Coast chlorites vary with temperature similarly to that reported in previous studies on diagenetic clays (e.g. Velde and Medhioub 1988; Hillier and Velde 1991; Jahren and Aagaard 1989; Jahren 1991; Jahren and Aagaard 1992), with the maximum Al_{total} and ^{IV}Al (mirrored by Si counter-variation) contents both showing an increase with temperature (Fig. 3). The linear evolution of maximum ^{IV}Al with temperature is from ~0.95-1.0 apfu at 100 °C to ~1.38-1.4 apfu at 216 °C (Fig. 3). On the contrary, ^{VI}Al shows no systematic evolution. Another obvious feature is the apparent decrease of octahedral vacancies with increasing temperature. This increase of trioctahedral character with *T* is a classical feature (e.g. Cathelineau 1988; Inoue et al. 2009), which suggests that, for each measured temperature, analyses with the highest octahedral occupancy represent the closest approach to the relevant equilibrium composition (as do highest-^{IV}Al analyses, Table 2). The "equilibrium" vacancy number is then observed to decrease from 0.3 apfu at 102 °C to 0.1 apfu at 232 °C. In contrast, no clear trend of the Fe + Mg content and XFe evolution with temperature is apparent. The compositional variations of chlorite discussed above can be explained by a combination of the Tschermak ($^{IV}Si^{VI}R^{2+} = {}^{IV}Al^{VI}Al$) and di-trioctahedral

226 substitutions ($2\ ^{VI}Al^{VI}\square = 3\ ^{VI}R^{2+}$), where $\square$ and R^{2+} represent octahedral vacancies and
227 divalent cations like Fe and Mg, respectively. Their combination in a 2 to 1 ratio would
228 account for the observed variations in ^{IV}Si, ^{IV}Al and vacancy, for the near constancy of ^{VI}Al,
229 and slight possible increase in R^{2+}. For the two samples at 204 and 232 °C, the ^{IV}Al and ^{VI}Al
230 contents are surprisingly low compared to the general tendency (Fig. 3 and Table 2), and are
231 compensated by large R^{2+} and Si contents. This may be due to a different precursor mineral, a
232 different bulk composition, an Al-poor rock composition or a non-equilibrated mineral
233 chemistry.

234 From these observations, the chemical variations with *T* and the differences between
235 crystal core and rim compositions (Fig. 1, 2 and 3) are clearly established at the nanoscale,
236 suggesting a chemical zonation of these phyllosilicates. This zonation can be the result of the
237 dissolution-reprecipitation process occurring along the crystal rims, in accordance to the *P*-*T*
238 conditions, in spite of the low-*T* nature of these phyllosilicates. In addition, the scattering in
239 the dataset observed at each temperature among the crystal-rim compositions (Fig. 2 and 3),
240 for both illite and chlorite, suggests that rim compositions do not all record the last, highest-
241 temperature equilibrium conditions, but that some of them were acquired during earlier stages
242 of equilibration during burial. Indeed, each rim composition refers to a specific part of the *P*-*T*
243 history of the crystal, i.e. the different compositions indicate the different steps of
244 crystallisation with *T* during the burial. As a consequence, only the "extreme" compositions
245 refer to the BHT-BHP. Owing to the difficulty to locate the rim areas that record the last and
246 higher-temperature equilibration, we have considered only the three or four analyses (when it
247 was possible), for each sample, that represent the compositions closest to equilibrium
248 compositions. This selection of such illite and chlorite rim analyses was used to test the
249 phyllosilicate-based thermobarometers.
250

Tested thermobarometers

Chlorite thermobarometry

The pioneer chlorite thermometer proposed by Cathelineau and Nieva (1985) and refined by Cathelineau (1988) is an empirical calibration based on a linear increase of ^{IV}Al content with temperature. Several authors (e.g. Shau et al. 1990; De Caritat et al. 1993; Jiang et al. 1994; Essene and Peacor 1995) have criticized the use of this equation as a thermometer, firstly because the chlorite analyses used for the equation calibration were suspected to be contaminated by other mineral phases, and secondly because the ^{IV}Al content of chlorite also depends on the bulk-rock composition. The latter point implies that the thermometer should not been used for other rock composition than the one used for its calibration. In order to take bulk-rock composition effects into account, several tentative corrections were introduced in various empirical equations, mainly based on the Fe/(Fe+Mg) ratio (Kranidiotis and McLean 1987; Jowett 1991; Hillier and Velde 1991; Zang and Fyfe 1995; Xie et al. 1997). All these equations are tested in this study and summarized in Table 3 and Appendix 4.

Alternatively, thermodynamic or semi-thermodynamic models were proposed by Walshe (1986), Vidal et al. (2005, 2006) and Inoue et al. (2009), to estimate *P*-*T* formation conditions from chlorite compositions, in most instances considering the chlorite+quartz equilibrium. These models differ by the choice of the end-member components and activity-composition relationships, and by the *P*-*T* data used to constrain the activity models (cf. Appendix 4). Moreover, Walshe (1986) and Inoue et al. (2009) neglected the non-ideal contributions and the effect of pressure, whereas Vidal et al. (2005) took them into account. According to the chlorite structure (Bailey 1988; Holland et al. 1998), two assumptions are also possible for the cationic mixing model: an ordered distribution, which was adopted by Vidal et al. (2005, 2006), or a random mixing, as used by Walshe (1986) and Inoue et al. (2009) (Table 3). In

order to test these models, we assumed that $a_{qz} = 1$ and $a_{H2O} = 1$, which is ensured by the presence of quartz and seems reasonable for low-*T* chlorite of diagenetic and hydrothermal origin (Inoue et al. 2009), and accounts for the low carbonate content in the rocks. In addition, and contrary to the empirical thermometers, these three thermodynamic models require an Fe^{3+} content estimate to be applied. In this study, $Fe^{3+}/\Sigma Fe$ ratios were estimated by the multi-equilibrium approach of Vidal et al. (2006).

K-deficient mica thermobarometry

Battaglia (2004) proposed an empirical illite thermometer directly based on K content with a correction accounting for the Fe-Mg content, which is considered as an indicator of the variation of rock composition. Besides, Parra et al. (2002) proposed and calibrated a thermodynamic model representing the phengite-quartz equilibrium, calculated from activity of chosen end-members and taking into account the non-ideal part of activity coefficients. Dubacq et al. (2010) extended this model to smectite, illite, interlayered smectite-illite and mica by considering the *T*–hydration relationship, the pressure and the rock composition, and using multi-equilibrium thermobarometry. This model was the first attempt to provide a unique set of 2:1 phyllosilicates thermodynamic properties in a solid-solution model relevant from diagenetic to metamorphic conditions. The model involves an assumed ordered cationic distribution and nine end-members (one of which has several levels of hydration), in order to cover the whole compositional space of 2:1 phyllosilicates (cf. Appendices 1 and 3). The Dubacq et al. (2010) model also considers the non-ideality of cationic exchanges and, on the basis of three independent equilibria and their hydrated equivalent for any smectite, illite or mica + quartz + water equilibrium, yields a pressure–temperature relation simultaneously with the hydration state (Table 3).

Illite-chlorite assemblages

With the high-spatial-resolution analytical protocol used in this study, we can target pairing of illite and chlorite analyses supposed to represent local equilibria. The relevant heterogeneous equilibrium was envisaged by Walshe (1986) as a thermometer, considering a chlorite + mica + quartz + K-feldspar + water assemblage. The author chose to represent the mica phase with a muscovite structure and a random-mixing cation distribution and ideal activities (cf. Appendix 4). This equilibrium was also used to justify the combination of Vidal et al. (2005, 2006) and Dubacq et al. (2010) models as a multi-equilibrium approach. In this case, the non-ideal ordered models for illite-micas (Dubacq et al. 2010) and chlorites (Vidal et al. 2005, 2006) can be used simultaneously to deduce *T* and *P*, assuming the achievement of local equilibrium between chlorites and illites. This is what has been tested and applied in this study to a series of Gulf Coast samples and summarized in Table 3.

P-T estimates from Gulf Coast phyllosilicates

Estimation of $Fe^{3+}/\Sigma Fe$ used to test thermobarometers

The chlorite thermodynamic thermobarometers need an estimation of $Fe^{3+}/\Sigma Fe$ ratios to be correctly applied. However, measuring the Fe^{3+} content at the nanoscale is challenging, even with the recent methods. For instance, the scanning transmission X-ray microscopy (STXM) and X-ray absorption near edge-structure (XANES) study of Bourdelle (2011, *PhD*) on Gulf Coast chlorites remains only qualitative. In order to circumvent the Fe^{3+} issue, Vidal et al. (2005) and Vidal et al. (2006) proposed a numerical method to estimate a minimum $XFe^{3+} = Fe^{3+}/\Sigma Fe$ based on the achievement of convergence of 4 reactions (chlorite+quartz and internal chlorite equilibria) at a given pressure, and a maximum XFe^{3+} when the equilibrium convergence is lost. Vidal et al. (2006) have shown on millimetre-size chlorites

that the minimum Fe^{3+} content calculated in this way was compatible with XANES measurements and can be used as an approximation of the actual Fe^{3+} content. Moreover, the difference between estimates of the minimum and maximum XFe^{3+} ratios is small in the low-*T* contexts. Therefore, we used the multi-equilibrium method proposed by Vidal et al. (2005, 2006) to estimate the $Fe^{3+}/\Sigma Fe$ ratio in Gulf Coast chlorites and used the results as input values in Vidal et al. (2005, 2006), Inoue et al. (2009) and Walshe (1986) models (where Fe^{3+} replaces ^{VI}Al). This estimated minimum $Fe^{3+}/\Sigma Fe$ was found to range between 0.1 and 0.45, which seems realistic for low-*T* chlorites (e.g. Inoue et al. 2009) and in agreement with literature data and our STXM-XANES qualitative study (Bourdelle 2011, *PhD*). We assumed that the Si > 3 apfu analyses, which are excluded by the models of Vidal et al. (2005) and Vidal et al. (2006), have the same XFe^{3+} ratio as the Si-poor analyses of the same sample. This assumption is supported by the consistency of the minimum XFe^{3+} values obtained for all the analyses (Si < 3 apfu) of any given sample. Even if these XFe^{3+} estimates are fraught with uncertainties, their input in the *T* calculations allows a sensitivity test of the various models with respect to XFe^{3+}.

Regarding the illite case, we do not have a numerical method to estimate the Fe^{3+} content. However, the qualitative XANES study of Bourdelle (2011, *PhD*) showed that 2:1 phyllosilicates of the Gulf Coast have a $Fe^{3+}/(Fe^{3+} + Fe^{2+})$ ratio higher than 50%. Because taking ferric iron into account implies an increase of calculated vacancies, the sensitivity of Dubacq et al. (2010) model to the XFe^{3+} had to be tested. This model was therefore applied to Gulf Coast illite under two limiting assumptions, with $XFe^{3+} = 0$ (case 1) and $XFe^{3+} = 0.7$ (case 2).

Results from Gulf Coast chlorites

In order to test the available chlorite thermometers, we have selected for each present-day *P* and *T* values only the three or four analyses that represent the closest approach to the relevant equilibrium composition, referred to as "maximum zoning composition". For the empirical thermometers, these are the highest-^{IV}Al analyses; for thermodynamic models, these are the extremum *log K* analyses (with > 80% overlap between the two sets), depending on the direction of the reaction.

The application of all the *empirical* chlorite thermometers according to measured temperature for the Gulf Coast samples shows that calculated *T* are systematically overestimated with respect to measured *T*. The thermometers of Cathelineau (1988), Kranidiotis and McLean (1987), Jowett (1991) and Xie et al. (1997) predict a maximum temperature of 360 ±20 °C for the measured temperature of 216 °C. These four different chlorite thermometers give similar results, showing the weak impact of the XFe corrections in the equations. Using the Zang and Fyfe (1995) equation, in which XFe has a stronger influence on the temperature estimation, the calculated temperatures are closer to measured temperatures, but still too high, e.g. 286 °C for a measured temperature of 216 °C. Hillier and Velde (1991) equation gives the closest, but the most scattered, temperature estimates to measured temperature, with results between 75 and 380 °C. Interestingly, their calibration is the only one that includes Gulf Coast chlorites (for which they pointed out the high ^{IV}Al content).

Temperature estimations obtained with the *thermodynamic* models of Walshe (1986), Inoue et al. (2009) and Vidal et al. (2005, 2006) models are represented on Figure 4, with all iron considered as Fe^{2+} (case 1) and with Fe^{3+} as obtained with Vidal et al. (2005, 2006) convergence method and assumed to replace ^{VI}Al (case 2).

In the case of $Fe_{total} = Fe^{2+}$, all the thermometers overestimate temperatures. Walshe (1986) thermometer gives a temperature trend between 205 °C and 323 °C for present-day

375 temperatures of 102 °C and 216 °C, respectively. Although the results obtained for samples at
376 204 °C and 232 °C are out of the general trend, this model overestimates systematically
377 temperatures by an average of ~70 °C — and excludes many Si-poor analyses (Si < 3 apfu)
378 due to inappropriate choice of end-members. The results obtained with Inoue et al. (2009)
379 method show a systematic trend of *T* overestimation by ~40 °C on the low-*T* side to ~70 °C
380 on the high-*T* side (Fig. 4). The model of Vidal et al. (2005, 2006), which excludes many
381 analyses (Si > 3 apfu), gives more scattered results but these are in better agreement with
382 measured temperatures and distributed on either side of the 1:1 line, with an average deviation
383 between calculated temperatures and BHT of 7 °C, against 65 °C and 59 °C for Inoue et al.
384 (2009) and Walshe (1986) models, respectively.

385 Taking into account the Fe^{3+} content, all thermodynamic models give lower or less
386 dispersed temperatures (Fig. 4). Regarding Vidal et al. (2005, 2006) model, the most visible
387 effect of the ferric iron is the narrowing of the data scatter. The calculated *T* values decrease
388 compared to the same dataset without Fe^{3+} content when they are higher than 150 °C, and
389 increase when they are below 150 °C. These trends were also noticed by Inoue et al. (2009) as
390 they tested the effect of Fe^{3+} on Vidal et al. (2001) model. Temperatures calculated with the
391 Walshe (1986) model are slightly but consistently lower when a minimum Fe^{3+} content is
392 considered, by about 15 °C on average. Maximum calculated temperatures range from 190 °C
393 to 308 °C for the present-day temperatures of 102 °C to 216 °C, respectively. The Fe^{3+}
394 content has a limited effect and the temperature overestimation persists. In the same way, the
395 results given by the thermometer of Inoue et al. (2009) are systematically lower when Fe^{3+}
396 content is considered, by about 20 °C on average, even if for a few analyses the shift can be as
397 large as 100 °C ($XFe^{3+} = 0.3$). New temperatures remain overestimated for most of them, for
398 instance they spread between 140°C and 181°C for a measured *T* of 102 °C, between 134 °C

399 and 285 °C for a measured *T* of 191 °C, and between 261 °C and 325 °C for a measured *T* of
400 216 °C.
401
402 **Results from Gulf Coast K-deficient micas**
403 As for chlorite, the available illite thermometers were tested using only the three or
404 four analyses that may be the closest to the "maximum zoning composition" for each present-
405 day *P* and *T*. For the empirical thermometers, these are the highest-K analyses; for
406 thermodynamic models, these are the extremum *log K* analyses (with > 85% overlap between
407 the two sets), depending on the direction of reaction.
408 The empirical illite thermometer (Battaglia, 2004) gives results that show a positive
409 correlation with the measured temperatures (Fig. 5), but with a systematic shift by an average
410 of about +40-50 °C at high *T* and about +60-70 °C at low *T*.
411 The thermodynamic model of Dubacq et al. (2010) yields for each analysis of illite in
412 equilibrium with quartz a *P*-*T*-*m*H_2O stability relation. In the present case, the measured
413 pressure was used as input value to calculate the temperature and hydration state. The results
414 obtained with $Fe_{total} = Fe^{2+}$ (Fig. 6) show that most calculated temperatures are slightly
415 overestimated (by less than 50 °C) and are less well correlated with measured *T* than with the
416 Battaglia (2004) thermometer. Maximum temperatures range from 165 °C to 256 °C for
417 measured 121 °C and 216 °C respectively, and 230 °C for measured 232 °C. If the
418 calculations are made assuming $XFe^{3+} = 0.7$ on the basis of preliminary STXM-XANES data,
419 the results show (Fig. 6) a very similar pattern of overestimation, but with a slightly wider
420 data scattering than with pure Fe^{2+}.
421
422 **Results from illite-chlorite assemblages**

To use illite + chlorite thermometers, three or four illite-chlorite pairs of rim analyses, located at less than 50 nm on either side of the illite-chlorite interface, were retained for each sample, whenever possible. When testing the effect of ferric iron, we used the same input data as above, i.e. XFe^{3+} ratio varying between 0.1 and 0.45 in chlorite as obtained with Vidal et al. (2005, 2006) method, and the fixed value of 0.7 in illite-like phases according to STXM-XANES results.

In the case of Walshe (1986) method, *log K* is negatively correlated with temperature, and the selected pairs are those yielding the lowest *log K* values. The reaction involved in Walshe (1986) calculation requires the presence of K-feldspar in the assemblage, which was observed by SEM in most of our samples. The resulting calculated temperatures show a positive correlation with the measured temperatures (Fig. 7), provided the 102 °C sample is considered as an outlier, but they are generally overestimated by ~0-60 °C. Results show a trend between 133-172 °C for a measured 121 °C to 272-320 °C for a measured 232 °C. The Fe^{3+} content has no effect as the corresponding temperatures differ from the previous ones by only 3 to 4 °C.

The results of the multi-equilibrium calculation based on Vidal et al. (2005, 2006) model and Dubacq et al. (2010) hydration model are shown in Figure 8. As consideration of Fe^{3+} was shown to hardly improve chlorite thermometry and to slightly affect illite thermometry with these database and solution models, only calculations with minimum XFe^{3+} are presented here. Unlike most other models, the calculated temperatures (calculation from BHP; Fig. 8-b) are not clearly overestimated, but are within ±50 °C of the measured temperatures. In contrast, the calculated pressures (Fig. 8-c) are not reliable, as they sometimes exceed 5 kbar, for a maximum measured value of 1.2 kbar.

Discussion

448

449 **The need for spatially highly resolved analyses and relevant analyses selection for clay**
450 **thermometry**

451 The fine-scale compositional variations of low-*T* chlorites and illites were studied on
452 diagenetic crystals as a function of increasing *P*-*T* conditions with a very high spatial control
453 on microtextural interactions. Using this protocol, the presence of an intra-crystalline
454 chemical zonation in low-*T* crystals was clearly established. The grain rims composition
455 seems to respond to the *P*-*T* variations and therefore to approach equilibrium while the crystal
456 core may preserve relic compositions. However, the dispersion at each temperature of crystal-
457 rim compositions, for both illite and chlorite, indicates that rim compositions do not all record
458 the last, highest-temperature equilibrium conditions but that some of them were acquired
459 during earlier stages of equilibration during burial. Thus, the selection of analyses becomes a
460 crucial point when trying to estimate the formation temperature and thermometry is not
461 straightforward because the composition of each part of a crystal may refer to one part of the
462 *P*-*T*/burial history. Using EMP would lead to average the crystal core-rim compositions, and
463 to a biased application of geothermobarometers. In this way, it is clear that the use of TEM,
464 with high spatial resolution, is highly recommended.

465

466 **Evaluation of clay minerals thermometry and Fe^{3+} effect**

467 In the chlorite case, the empirical approaches based on the aluminum content
468 (Cathelineau 1988; Kranidiotis and McLean 1987; Jowett 1991; Hillier and Velde 1991; Zang
469 and Fyfe 1995; Xie et al. 1997) give disparate temperatures and overestimate the temperature
470 of our Gulf Coast samples by up to 170°C with respect to BHT, taken as indicative of the
471 maximum burial conditions insofar as the subsidence has been continuous since the
472 Cretaceous. In contrast, the temperature estimated with the models of Vidal et al. (2005,

2006) and Inoue et al. (2009) [as well as the chlorite + mica + K-feldspar + quartz + water equilibrium of Walshe (1986)] are in fair agreement with the BHT. This difference in the results between empirical calibrations and thermodynamic approaches suggests that empirical chlorite thermometers are inaccurate, most likely because of their inability to account properly for bulk-rock compositional effects. This conclusion is in line with the results of earlier studies by De Caritat et al. (1993) and Essene and Peacor (1995), which concluded that the empirical thermometers based on the ^{IV}Al content of chlorite are inaccurate and should be used with caution. In this context, the use of a spatially highly resolved analytical approach cannot help to improve the results.

The temperatures estimated from chlorite compositions with the non-empirical thermodynamic approach of Vidal et al. (2005, 2006) are in better agreement with the BHT, but the calculated temperatures are slightly scattered. Moreover, the numerous chlorite analyses showing high Si content (> 3 apfu) cannot be handled with this model. The semi-empirical approaches proposed by Walshe (1986) and especially by Inoue (2009) yield temperature estimates higher than but still in reasonable agreement with the BHT. As in the case of Vidal et al. (2005, 2006) model, the Walshe (1986) formalism cannot handle all the chlorite compositions measured in our samples, and is limited to chlorite with Si > 3 pfu. Only the formalism of Inoue et al. (2009) can be used for the entire set of compositions measured for Gulf Coast samples.

The present study also shows the strong effect of the distinction between Fe^{3+} and Fe^{2+} (Fig. 4) and confirms previous observations (Vidal et al. 2006; Inoue et al. 2009). The consideration of Fe^{3+} content increases the number of octahedral vacancies and reduces the R^{2+} occupancy. As octahedral vacancy (sudoite content and activity) is negatively correlated with *T*, the reduced R^{2+} occupancy generally results in a lower calculated temperature. However, the temperature variation due to the introduction of Fe^{3+} content is different for

each thermometer. Inoue et al. (2009) model is the most sensitive to ferric iron (Fig. 4), with a *T* variation between cases 1 and 2 ranging from 7 to 108 °C, compared to 6-49 °C for Walshe (1986) model and 0-59 °C for Vidal et al. (2005; 2006) model (Fig. 4). The choice of a random-mixing repartition of cations in the model of Inoue et al. (2009) seems to be the reason for this difference, because the vacancy number has a greater weight in the *log K* calculation of random-mixing models than in the ordered model. Surprisingly, Vidal et al. (2005, 2006) model is the only one for which Fe^{3+} consideration increases the calculated temperatures at low-*T* and decreases them at high-*T*. In summary, all the thermodynamic models give overestimated and scattered temperatures if all iron is assumed as ferrous; taking into account a minimum Fe^{3+} occupancy leads to reduce the overestimation, whereas the results still remain slightly scattered. The valence state of iron is therefore not the sole reason for the inaccuracy of chlorite thermodynamic thermometers.

The observed scatter of results can be due to some errors, which stem from the uncertainties in BHT, in the thermodynamic standard-state properties of the end-members and solution models, departure of the analysed compositions from equilibrium compositions, and analytical uncertainties. The source of error resulting from the uncertainties associated with the thermodynamic data is difficult to estimate, because the thermodynamic data used for example by Vidal et al. (2005, 2006) model were calibrated using experimental and natural data of various levels of confidence. However, it is likely that the uncertainties in the thermodynamic data have a systematic effect on the calculated locations of the chlorite+quartz equilibrium. Moreover, the uncertainties in the thermodynamic data cannot be put forward in the case of Inoue et al. (2009) model, which is semi-empirical and not based on thermodynamic properties.

Even if the thermodynamic data were perfect, imprecision in the analysed compositions of minerals places limits on the accuracy with which *T* can be known. The scatter resulting from

523 the variation of the chlorite compositions within specific bounds given by the precision of the
524 TEM analysis (element-dependent) can be calculated with a Monte Carlo technique
525 (Lieberman and Petrakakis 1991). Thus, the effect of analytical uncertainties was simulated
526 (i) to confirm that the observed compositional variations are significant and not due to the
527 inaccuracy of analyses and (ii) to compare the accuracy of each thermometer by the
528 evaluation of the sensitivity of the equilibrium *K* constant calculation to a slight variation of
529 composition. In this MonteCarlo study, we focussed on the chlorite models of Walshe (1986),
530 Vidal et al. (2005, 2006) and Inoue et al. (2009) because they yield similar thermometric
531 results and so could be distinguished by their precision, i.e. their sensitivity to the error
532 factors. Starting from three Gulf Coast chlorite compositions (at 129, 204 and 232 °C as
533 example), a Gaussian error distribution with $1\sigma = 1\%$ relative for all oxides was randomly
534 sampled around the nominal weight percentage for each oxide in chlorite. This deviation of
535 1% for each oxide from the nominal composition was assumed to represent the TEM
536 analytical uncertainties (as Vidal and Parra, 2000); 250 permutations led to the simulation of
537 250 mineral compositions. The set of simulated chlorite compositions was used to calculate
538 250 separate temperatures (noted "simulated temperatures"); Fe^{3+} content was recalculated
539 each time. The maximum permissible scatter from the 'nominal' temperature estimate (from
540 nominal chlorite) was fixed to a 95% confidence level. Indeed, 238 of the 250 simulated
541 temperatures represent the assumed maximum temperature scatter, and therefore the influence
542 of analytical uncertainties on temperature calculation. Results are presented in Figure 9. The
543 observed variations of chemical compositions (Fig. 2 and 3) and the resulting variations of
544 temperature estimates are clearly one order of magnitude larger than the possible effect of
545 analytical uncertainties. For Walshe (1986) model, 95% of simulated temperatures are
546 separated by less than 10.7, 12.1 and 12.8 °C from the three nominal temperature estimates
547 (190, 185 and 184 °C), respectively (Fig. 9). For Vidal et al. (2005, 2006) model, the absolute

548 deviation is slightly higher than for the Walshe (1986) model, with 95% of simulated
549 temperatures separated by less than 19, 17.4 and 14.8 °C from nominal temperature estimates
550 (132, 211, 203 °C), respectively (Fig. 9). Finally, the higher absolute deviation of simulated
551 temperatures is obtained for the Inoue et al. (2009) model, with 95% of simulated
552 temperatures separated by a maximum of 15.7, 26.8 and 26.0 °C from nominal temperature
553 estimates (143, 234, 235 °C), respectively (Fig. 9). These results show that the thermometer
554 of Inoue et al. (2009) is the most sensitive to compositional variations, involving a
555 dependence between the accuracy of analyses and that of the temperature calculation.
556 Therefore, the relative accuracy (noted RA; RA = absolute deviation represented by 95% of
557 simulated temperatures x 100 / Estimated *T*) of the Inoue thermometer is consistently higher
558 by more than 10.9%, whereas Vidal et al. (2005, 2006) model has a RA < 8.2% (excepted for
559 BHT = 129 °C) and Walshe (1986) model has a RA < 7% (Fig. 9). Paradoxically, we observe
560 that Walshe (1986) proposed a geothermometer with a very good reproducibility of estimates,
561 but with a very rough accuracy. In fact, the best compromise between sensitivity to analytical
562 uncertainties and accuracy of temperature is given by Vidal et al. (2005, 2006) model.
563
564 In the illite case, the empirical thermometer of Battaglia (2004) gives temperatures
565 overestimated compared to the present-day temperatures. Remarks made against chlorite
566 empirical thermometers are also valid in the illite case. Moreover, the equation correction
567 involving |Fe-Mg|, as proposed by Battaglia (2004), has no crystal-chemical basis.
568 The temperatures estimated with the model of Dubacq et al. (2010) show the same increasing
569 trend as measured temperatures and are not excessively scattered, especially at "high"-*T* (>
570 180 °C). At lower temperature, the calculated temperatures may be overestimated by more
571 than 50°C, but not systematically. This may be due to the difficulty to take into account
572 purely potassic, charge-deficient 2:1 phyllosilicates at low-*T*. The addition of Fe^{3+} content

573 deteriorates the correlation, and the estimated temperatures are slightly increased and
574 scattered, involving a recommendation for a pure-Fe^{2+} application as mentioned by the
575 authors.
576
577 Concerning the illite-chlorite assemblage, the Walshe (1986) formalism for chlorite +
578 mica + quartz + K-feldspar + water equilibrium yields calculated temperatures that are
579 positively correlated with measured *T* (Fig. 7). For $Fe_{total} = Fe^{2+}$, this model allows one to
580 obtain results with a better accuracy (50 °C on average) than those obtained with Walshe's
581 chlorite + quartz thermometer, and the addition of Fe^{3+} content changed the calculated *T* by
582 only ~4 °C. The 'multi-equilibrium' approach combining Vidal et al. (2006) model for
583 chlorite and Dubacq et al. (2010) model for smectite-illite-phengite gives plausible
584 temperatures (Fig. 8): all temperatures boxes overlap the shaded area of BHT ± 50°C.
585 However, several estimates yield too high temperatures, such as samples at 216 °C (BHT) for
586 which calculated *T* is overestimated, or one sample at 191 °C (BHT), for which the calculated
587 *T* range is large (up to 339 °C). Nevertheless, the 'multi-equilibrium approach', combined to
588 the fine-scale analytical protocol, gives satisfactory temperature estimates, showing the
589 importance of analyses selection.
590 In summary, the two illite + chlorite models tested here give reliable results. In fact, the
591 protocol enables to measure equilibrium compositions of both illite and chlorite at the
592 nanoscale. These results suggest that it is likely the scale at which the heterogeneous
593 equilibrium illite + chlorite is achieved. This allows for relating the different equilibrium
594 compositions and gives a good basis for thermobarometry at low temperature.
595

596 **Chlorite and illite barometry**

597 The thermodynamic model of Vidal et al. (2005, 2006) is the only chlorite-based
598 model to consider the pressure parameter. Applied to metamorphic rocks, it has shown the
599 importance of pressure on the chemical composition variations (e.g. Malasoma and Marroni,
600 2007). However, in a low-*P*/low-*T* diagram, the equilibrium curves calculated from our
601 chlorite analyses are almost parallel to the *P* axis, which means that the chemical variations in
602 chlorite are essentially dependent on temperature, thus confirming the validity of Inoue et al.
603 (2009) assumption. The model of Dubacq et al. (2010) considers the pressure as a significant
604 parameter for the case of illite. Unlike the chlorite + quartz equilibrium curve, the illite +
605 quartz equilibrium curve is not parallel to the *P* axis, and is *P*-*T*-dependent. However, the
606 *dP/dT* slope of this curve is steep, and for the *P*-*T* domain investigated in this study, the
607 model of Dubacq et al. (2010) predicts a higher *T*-dependence than *P*-dependence for illite
608 composition. Moreover, the pressure uncertainty is as large as the entire range of pressure
609 variations in diagenesis, which precludes any reliable estimate. Similarly, the pressure
610 conditions constrained by the chlorite + illite equilibrium remain uncertain (Fig. 8-c), because
611 of the steep slope of the illite + quartz equilibrium curve: except for one sample at 1.05 kbar
612 (BHP), all measured pressures are located in the calculated pressure ranges, but these ranges
613 are large (up to 11 kbar). In fact, the pressure effect on the low-*T* phyllosilicates appears to be
614 too low compared to the temperature impact in this realm, involving a relative failure of the
615 barometers to give results with acceptable error deviation.
616
617 **Conclusion**
618
619 The analytical protocol proposed by Bourdelle et al. (2012) makes it possible to obtain
620 data at nanometer scale and to distinguish crystal-rim and -core analyses, allowing one to
621 analyse the illite-chlorite interfaces and the calculation of illite-chlorite equilibrium. In fact,

622 the difference of chemical composition between rims and cores may be very significant, in
623 particular for the illite K content. Moreover, these chemical parameters generally show a *T*-
624 dependence that is the base of many thermometers, making the consideration of chemical
625 zonation a crucial point. In this respect, the present study showed the difference of impact and
626 reliability for the two variables: temperature and pressure. The pressure does not affect the
627 chlorite, but the illite composition. From the results of Vidal et al. (2005, 2006) and Dubacq et
628 al. (2010) models, the chlorite + quartz equilibrium seems to be essentially *T*-dependent at
629 low grade, whereas the illite + quartz equilibrium is influenced by both temperature and
630 pressure. However, if the *T* estimate is realistic, the *P* prediction remains difficult and
631 inaccurate.
632 Nevertheless, from a thermometric point of view, empirical and thermodynamic approaches
633 lead to disparate results. The empirical chlorite thermometers all overestimate the temperature
634 of the studied samples, because the *T*-dependent ^{IV}Al or K variation alone is not an exclusive
635 quantitative relation, and the common correction, based on XFe, does not improve the
636 situation. The results of thermodynamic models are generally much more realistic (e.g. Vidal
637 et al. 2005, 2006; Inoue et al. 2009; Dubacq et al. 2010 [in particular for $T > 180$ °C], Walshe,
638 1986 [for the chlorite + mica + quartz + K-feldspar + water equilibrium], and multi-
639 equilibrium illite + chlorite approach), but revealed the importance of taking into account the
640 Fe^{3+} content, in particular in the case of chlorite disordered models.
641 The main difference between the semi-empirical or non-empirical thermodynamic and the
642 empirical approaches is that the former are based on the ratio of chlorite end-members
643 activities (equilibrium constant *K*). The same *log K*, and therefore the same temperature
644 estimate can be obtained for chlorites of different compositions. Such approaches are thus
645 compatible with the observation that chlorites crystallizing at the same temperature in rocks
646 of different bulk compositions have different compositions. In contrast, such observation

cannot be accounted for by the empirical thermometers based on the ^{IV}Al content, even corrected using the Mg and Fe content (e.g. Karnidiotis and McLean 1987). Moreover, thermodynamic models make possible illite + chlorite thermometry in the low-*T* domain. Therefore, the chlorite + mica + quartz + K-feldspar + water thermometer proposed by Walshe (1986) and the combination of Dubacq et al. (2010) and Vidal et al. (2005, 2006) models give satisfactory results on Gulf Coast phyllosilicates, suggesting local equilibrium between illite and chlorite along crystal rims. The prerequisite for such results is that thermodynamic models are combined with an analytical technique that can resolve the very fine-scale compositional readjustments or overgrowths that may witness an approach of local equilibrium and keep record of it. However, the choice of end-members for thermodynamic models can become a limitation depending on the composition domain studied. Indeed, the models of Vidal et al. (2005, 2006) and Walshe (1986) have the drawback to exclude many chlorite analyses with Si content higher or less than 3 apfu, respectively, which is unfortunately a common case for low-*T* chlorites.

Altogether, the thermodynamic approaches, based on the ratio of chlorite end-members activities, are compatible with the observation that chlorites crystallizing at the same temperature in rocks of different bulk compositions have different compositions. This study however stresses that recent models yield accurate results only if the compositional data used consider the chemical intracristalline zonation occurring in low-*T* clay crystals. This requires the use of nanoscale chemical analysis.

Acknowledgements

We are most grateful to the materials characterization department of IFP Energies nouvelles-Lyon, in particular to F. Moreau, and to the laboratory of CP2M-Université Aix-Marseille, for technical advice. Thanks are also extended to K. Milliken, S. Dutton and J. Donnelly of Bureau of Economic Geology at Austin. The discussions and comments of the journal editor R. Yuretich and of P. Aagaard are gratefully acknowledged. This study was financially supported by IFP Energies nouvelles, CNRS and ENS Paris.

References

Bailey, S.W. (1988) Chlorites: structures and crystal chemistry. In S.W. Bailey, Eds., Hydrous Phyllosilicates (Exclusive of Micas), p. 347-403. Mineralogical Society of America, Washington D.C.

Battaglia, S. (2004) Variations in the chemical composition of illite from five geothermal fields: a possible geothermometer. Clay Minerals, 39, 501-510.

Bebout, D.G., Weise, B.R., Gregory, A.R., and Edwards, M.B. (1982) Wilcox sandstone reservoirs in the deep subsurface along the Texas Gulf Coast. 125 p. University of Texas, Austin.

Bodner, D.P. (1985) Heat variations caused by groundwater flow in growth faults of the South Texas, Gulf Coast basin, 187 p. Ph.D. thesis, University of Texas, Austin.

Bodner, D.P. and Sharp, J.M. (1988) Temperature variations in South Texas subsurface. American Association of Petroleum Geologists Bulletin, 72, 21-32.

Bourdelle, F. (2011) Thermobarométrie des phyllosilicates dans les séries naturelles: Conditions de la diagenèse et du métamorphisme de bas degré, 318 p. Ph.D. thesis, University Paris-Sud, Orsay.

Bourdelle, F., Parra, T., Beyssac, O., Chopin, C., and Moreau, F. (2012) Ultrathin section preparation of phyllosilicates by Focused Ion Beam milling for quantitative analysis by TEM-EDX. Applied Clay Science, 59-60, 121-130.

Cathelineau, M. (1988) Cation site occupency in chlorites and illites as a function of temperature. Clay Minerals, 23, 471-485.

Cathelineau, M. and Nieva, D. (1985) A chlorite solid solution geothermometer. The Los Azufres (Mexico) geothermal system. Contributions to Mineralogy and Petrology, 91, 235-244.

De Caritat, P., Hutcheon, I., and Walshe, J.L. (1993) Chlorite geothermometry: a review. Clays and Clay Minerals, 41, 219-239.

Dodge, M.M. and Posey, J.S. (1981) Structural cross sections, Tertiary formations, Texas Gulf Coast. University of Texas, Austin.

Dubacq, B., Vidal, O., and De Andrade, V. (2010) Dehydration of dioctahedral aluminous phyllosilicates: thermodynamic modelling and implications for thermobarometric estimates. Contributions to Mineralogy and Petrology, 159, 159-174.

Dutton, S.P. and Loucks, R.G. (2010) Diagenetic controls on evolution of porosity and permeability in lower Tertiary Wilcox sandstones from shallow to ultradeep (200-6700 m) burial, Gulf of Mexico Basin, USA. Marine and Petroleum Geology, 27, 69-81.

Essene, E.J. and Peacor, D.R. (1995) Clay mineral thermometry - A critical perspective. Clays and Clay Minerals, 43, 540-553.

Heaney, P.J., Vicenzi, E.P., Giannuzzi, L.A., and Livi, K.J.T. (2001) Focused ion beam milling: A method of site-specific sample extraction for microanalysis of Earth and planetary materials. American Mineralogist, 86, 1094-1099.

718 Helgeson, H.C., Delany, J.M., Nessbitt, H.W., and Bird, D.K. (1978) Summary and critique
719 of the thermodynamic properties of rock-forming minerals. American Journal of Science,
720 278A, 1-229.
721 Helgeson, H.C and Aagaard, P. (1985) Activity/composition relations among silicates and
722 aqueous solutions. I. Thermodynamics of intrasite mixing and substitutional order/disorder in
723 minerals. American Journal of Science, 285, 769-844.
724 Hillier, S. and Velde, B. (1991) Octahedral Occupancy and the Chemical-Composition of
725 Diagenetic (Low-Temperature) Chlorites. Clay Minerals, 26, 149-168.
726 Holland, T.J.B., Baker, J., and Powell, R. (1998) Mixing properties and activity composition
727 relationships of chlorites in the system MgO-FeO-Al_2O_3-SiO_2-H_2O. European Journal of
728 Mineralogy, 10, 395-406.
729 Hutcheon, I. (1990) Clay carbonate reactions in the Venture area, Scotian Shelf, Nova Scotia,
730 Canada. The Geochemical society, Special Publication, 2, 199-212.
731 Inoue, A., Meunier, A., Patrier-Mas, P., Rigault, C., Beaufort, D., and Vieillard, P. (2009)
732 Application of Chemical Geothermometry to Low-Temperature Trioctahedral Chlorites.
733 Clays and Clay Minerals, 57, 371-382.
734 Jahren, J.S. (1991) Evidence of Ostwald ripening related recrystallization of chlorites from
735 reservoir rocks offshore Norway. Clay Minerals, 26, 169-178.
736 Jahren, J.S. and Aagaard, P. (1989) Compositional variations in diagenetic chlorites and
737 illites, and relationships with formation-water chemistry. Clay Minerals, 24, 157-170.
738 Jahren, J.S. and Aagaard, P. (1992) Diagenetic Illite-Chlorite Assemblages in Arenites .1.
739 Chemical Evolution. Clays and Clay Minerals, 40, 540-546.
740 Jiang, W.T., Peacor, D.R., and Buseck, P.R. (1994) Chlorite Geothermometry -
741 Contamination and Apparent Octahedral Vacancies. Clays and Clay Minerals, 42, 593-605.

Jones, P.H. (1975) Geothermal and hydrocarbon regimes, Northern Gulf of Mexico basin. In M.H. Dorfman and R.W. Deller, Eds., Proceedings of the first geopressured geothermal energy conference, p. 15-89. University of Texas, Center for energy studies, Austin.

Jowett, E.C. (1991) Fitting iron and magnesium into the hydrothermal chlorite geothermometer. GAC/MAC/SEG Joint annual meeting, Toronto, Canada.

Kehle, R.O. (1971) Geothermal survey of North America. Annual progress report, American Association of Petroleum Geologists, 31 p.

Kohler, E., Parra, T., and Vidal, O. (2009) Clayey Cap-Rock Behavior in H_2O-CO_2 Media at Low Pressure and Temperature Conditions: An Experimental Approach. Clays and Clay Minerals, 57, 616-637.

Kosters, E.C., Bebout, D.G., Seni, S.J., Garrett, C.M., Brown, L.F., Hamlin, H.S., Dutton, S.P., Ruppel, S.C., Finley, R.J., and Tyler, N. (1989) Atlas of major Texas gas reservoirs. 168 p. University of Texas, Austin.

Kranidiotis, P. and McLean, W.H. (1987) Systematics of chlorite alternation at the Phelps Dodge massive sulfide deposit, Matagami, Quebec. Economic Geology, 82, 1898-1911.

Lanson, B. and Besson, G. (1992) Characterization of the End of Smectite-to-Illite Transformation - Decomposition of X-Ray-Patterns. Clays and Clay Minerals, 40, 40-52.

Lieberman, J. and Petrakakis, K. (1991) TWEEQU Thermobarometry: Analysis of uncertainties and application to granulites from western Alaska and Austria. Canadian Mineralogist, 29, 857-887.

Loucks, R.G., Dodge, M.M., and Galloway, W.E. (1979) Sandstone consolidation analysis to delineate areas of high-quality reservoirs suitable for production of geopressured geothermal energy along the Texas Gulf Coast. 97 p. U.S. Department of energy, Austin.

765 Lynch, F.L. (1994) The effects of depositional environment and formation water chemistry on
766 the diagenesis of Frio formation (Oligocene) sandstones and shales, Aransas, Nueces and San
767 Patricio counties, Texas, 303 p. Ph.D. thesis, University of Texas, Austin.
768 Malasoma, A. and Marroni, M. (2007) HP/LT metamorphism in the Volparone Breccia
769 (Northern Corsica, France): evidence for involvement of the Europe/Corsica continental
770 margin in the Alpine subduction zone. Journal of Metamorphic Geology, 25, 529-545.
771 Mathieu, Y. and Velde, B. (1989) Identification of thermal anomalies using clay mineral
772 composition. Clay Minerals, 24, 591-602.
773 McKenna, T.E. (1997) Geologic and hydrologic constraints on fluid and heat flow in
774 overpressured rocks of the Rio Grande embayement, Gulf of Mexico basin, 241 p. Ph.D.
775 thesis, University of Texas, Austin.
776 Nunn, J.A. (1984) Subsidence and temperature histories for Jurassic sediments in the
777 Northern Gulf Coast: A thermal mechanical model. In D.G. Bebout, W.P.S. Ventress, B.F.
778 Perkins and C.H. Moore, Eds., The Jurassic of the Gulf rim, p. 309-322. GCSSEPM
779 Foundation 3th Annual Research Conference Proceedings, Houston, Texas.
780 Parra, T. (2001) Les équilibres chlorite-phengite : de l'étude de la lame mince aux calculs des
781 trajets pression-température, 391 p. Ph.D thesis, Université Paris-Sud XI, Orsay.
782 Parra, T., Vidal, O., and Agard, P. (2002) A thermodynamic model for Fe-Mg dioctahedral K
783 white micas using data from phase-equilibrium experiments and natural pelitic assemblages.
784 Contributions to Mineralogy and Petrology, 143, 706-732.
785 Perry, E.A. and Hower, J. (1970) Burial diagenesis in Gulf Coast pelitic sediments. Clays and
786 Clay Minerals, 18, 165-177.
787 Pfeiffer, D.S. (1989) Temperature variations and their relation to groundwater flow, South
788 Texas, Gulf Coast basin, 198 p. Ph.D. thesis, University of Texas, Austin.

789 Posey, J.S. (1986) The Louann Salt of the Gulf Coast basin, with emphasis on South Texas. In
790 W.L. Stapp, Eds., Contributions to the geology of South Texas, p. 440-446. South Texas
791 Geological Society, San Antonio.
792 Royden, L., Sclater, J.G., and Von Her, R.P. (1980) Continental margin subsidence and heat
793 flow: important parameters in formation of petroleum hydrocarbons. American Association of
794 Petroleum Geologists Bulletin, 64, 173-187.
795 Shau, Y.H., Peacor, D.R., and Essene, E.J. (1990) Corrensite and mixed-layer
796 chlorite/corrensite in metabasalt from northern Tawaïn: TEM/AEM, EMPA, XRD and optical
797 studies. Contributions to Mineralogy and Petrology, 105, 123-142.
798 Stanley, S.M. (1986) Earth and life through time, 689 p. New York.
799 Trotet, F., Vidal, O., and Jolivet, L. (2001) Exhumation of Syros and Sifnos metamorphic
800 rocks (Cyclades, Greece): new constraints on the P-T paths. European Journal of Mineralogy,
801 13, 901-920.
802 Van Cappellen, E. and Doukhan, J.C. (1994) Quantitative Transmission-X-Ray Microanalysis
803 of Ionic Compounds. Ultramicroscopy, 53, 343-349.
804 Velde, B. and Medhioub, M. (1988) Approach to chemical equilibrium in diagenetic chlorites.
805 Contributions to Mineralogy and Petrology, 98, 122-127.
806 Vidal, O., De Andrade, V., Lewin, E., Munoz, M., Parra, T., and Pascarelli, S. (2006) P-T-
807 deformation-Fe^{3+}/Fe^{2+} mapping at the thin section scale and comparison with XANES
808 mapping: application to a garnet-bearing metapelite from the Sambagawa metamorphic belt
809 (Japan). Journal of Metamorphic Geology, 24, 669-683.
810 Vidal, O., Goffe, B., Bousquet, R., and Parra, T. (1999) Calibration and testing of an
811 empirical chloritoid-chlorite Mg-Fe exchange thermometer and thermodynamic data for
812 daphnite. Journal of Metamorphic Geology, 17, 25-39.

Vidal, O. and Parra, T. (2000) Exhumation paths of high-pressure metapelites obtained from local equilibria for chlorite-phengite assemblages. Geological Journal, 35, 139-161.

Vidal, O., Parra, T., and Trotet, F. (2001) A thermodynamic model for Fe-Mg aluminous chlorite using data from phase equilibrium experiments and natural pelitic assemblages in the 100 ° to 600 °C, 1 to 25 kb range. American Journal of Science, 301, 557-592.

Vidal, O., Parra, T., and Vieillard, P. (2005) Thermodynamic properties of the Tschermak solid solution in Fe-chlorite: Application to natural examples and possible role of oxidation. American Mineralogist, 90, 347-358.

Walshe, J.L. (1986) A six-component chlorite solid solution model and the conditions of chlorite formation in hydrothermal and geothermal systems. Economic Geology, 81, 681-703.

Wirth, R. (2004) Focused Ion Beam (FIB): A novel technology for advanced application of micro- and nanoanalysis in geosciences and applied mineralogy. European Journal of Mineralogy, 16, 863-876.

Xie, X.G., Byerly, G.R., and Ferrell, R.E. (1997) IIb trioctahedral chlorite from the Barberton greenstone belt: Crystal structure and rock composition constraints with implications to geothermometry. Contributions to Mineralogy and Petrology, 126, 275-291.

Zang, W. and Fyfe, W.S. (1995) Chloritization of the Hydrothermally Altered Bedrock at the Igarape-Bahia Gold Deposit, Carajas, Brazil. Mineralium Deposita, 30, 30-38.

Figure captions

Figure 1: Analysis of an illite-like - chlorite assemblage, sample of Alamo#1 well, 5825 m. (a) SEM image of the petrographic thin section showing the emplacement of the FIB foil to be cut across the illite-like - chlorite interface. (b) Brigh-field TEM image of the FIB foil extracted from the section, with the platinium strap on top of it. (c) Enlargement with

838 exaggerated image contrast in order to show the analysis points. Note their size as compared
839 to scale bar, and their distribution. Analyses 1 to 9 are considered as rim analyses [white text],
840 all others as core analyses [black text]. K contents are indicated for illite-like phase in apfu [in
841 boxes]. Note the K content variation between crystal core and crystal rim.
842
843 Figure 2: K contents of 2:1 phyllosilicates of Gulf Coast *versus* measured temperatures
844 (corrected bottom-hole temperature, BHT). Comparison of crystal-rim and crystal-core
845 analyses. The outlined area enclosed within dashed bands qualitatively underlines the trend
846 drawn approximately by the "maximum illitization", i.e. rims analyses which were assumed
847 to represent the closest approach to relevant equilibrium composition.
848
849 Figure 3: ^{IV}Al contents of Gulf Coast chlorites *versus* measured temperatures (corrected
850 BHT). Comparison of crystal-rim and crystal-core analyses. The outlined area enclosed
851 within dashed band, qualitatively underlines the trend drawn approximately by the maximum
852 ^{IV}Al content in crystal-rims, which is assumed to represent the closest approach to relevant
853 equilibrium composition. Rectangles represent the difference between the maximum ^{IV}Al
854 content in rims and cores of chlorite grains.
855
856 Figure 4: Comparison between measured temperatures (corrected BHT with an assumed error
857 of 20 °C) and temperatures calculated with (a) Vidal et al. (2005, 2006) model, (b) Inoue et al.
858 (2009) model and (c) Walshe (1986) model. Solid symbols, $Fe_{total} = Fe^{2+}$; open symbols, Fe^{3+}
859 is considered (see text).
860

Figure 5: Comparison between measured temperatures (corrected BHT) and temperatures calculated with the empirical equation of Battaglia (2004). All Fe is considered as Fe^{2+}. Corrected BHT are represented with an assumed uncertainty of 20 °C.

Figure 6: Comparison between measured temperatures (corrected BHT) and temperatures calculated with the thermodynamic model of Dubacq et al. (2010). Solid symbols: Fe_{total} = Fe^{2+}; open symbols: Fe^{3+} content is considered (see text). Corrected BHT are represented with an assumed uncertainty of 20 °C.

Figure 7: Comparison between measured temperatures (corrected BHT) and temperatures calculated with the model of Walshe (1986) for the equilibrium chlorite + illite + K-feldspar + quartz + water. All Fe is considered as Fe^{2+}. Corrected BHT are represented with an assumed uncertainty of 20 °C.

Figure 8: Temperatures and pressures obtained from the combination of the non-ideal ordered models of Vidal et al. (2005, 2006) and Dubacq et al. (2010) for Gulf Coast chlorites. (a) Example of equilibrium convergence for several chlorite and illite analyses of one Gulf coast FIB section. The square area represents the *P-T* domain of convergence. All chl-ill analysis pairs are used. (b) Calculated temperatures compared to measured temperatures. Square areas correspond to [in abscissa] the assumed uncertainty of 20 °C in BHT data, [in ordinate] the maximum and the minimum temperatures obtained from the convergence domain (defined from all chl-ill analysis pairs of all FIB sections for each *P-T* data). (c) Calculated pressures compared to measured pressures. Square areas correspond to [in abscissa] the assumed uncertainty of ±100 bars in BHP data, [in ordinate] the maximum and the minimum pressures

obtained from the convergence domain (defined from all chl-ill analysis pairs of all FIB sections for each *P-T* data).

Figure 9: Results in terms of temperature of the Monte-Carlo simulation for the three studied chlorite thermometers (Walshe, 1986; Inoue et al., 2009; Vidal et al., 2005 2006), for three nominal chlorites (at BHT = 129, 204 and 232 °C). The areas represent the assumed uncertainty of ±20 °C on BHT in abscissa and the absolute accuracy obtained from a Monte-Carlo randomization on 250 chlorite compositions, with a 95% confidence level, in ordinate. Relative accuracy corresponds to absolute deviation x 100 / Estimated *T*.

Tables

Table 1: Selection of TEM-EDX analyses of Gulf Coast K-deficient mica: crystal rim analyses with the highest K content for each *P-T*. Atomic contents are given in atoms per formula unit (O = 11 apfu), and M1, M2 and M3 represent the cationic sites as defined by Dubacq et al. (2010). All iron is considered as ferrous.

Samples	AZ#159 9230	ST#470 10717	CK#2 12196	LA#1 13559	ST#356 14501	CW#1 14277	WR#C1 17805	FR#1 18946	AL#1 19110	AL#1 20711
Analysis	m42	m24	m24	m30	m13	m2	m33	m3	m34	m30
BHT (°C)	102	121	135	149	166	191	191	204	216	232
BHP (bars)	300	590	690	850	800	750	1050	1150	1150	1200
Si	3.38	3.78	3.44	3.41	3.10	3.43	3.37	3.30	3.18	3.32
Ti	0.01	0.01	0.01	0.02	0.02	0.00	0.03	0.02	0.00	0.02
^{IV}Al	0.62	0.21	0.55	0.58	0.89	0.57	0.59	0.68	0.82	0.66
^{VI}Al	1.87	1.53	1.82	1.75	1.86	1.90	1.48	1.57	1.74	1.59
ΣAl	2.48	1.74	2.37	2.32	2.75	2.46	2.07	2.25	2.56	2.25
ΣFe^{2+}	0.07	0.20	0.10	0.11	0.16	0.14	0.35	0.26	0.30	0.23
ΣMg	0.11	0.32	0.14	0.18	0.14	0.06	0.31	0.27	0.15	0.20
Mg (M1)	0.03	0.03	0.03	0.02	0.08	0.03	0.06	0.05	0.06	0.01
Fe^{2+} (M1)	0.02	0.02	0.02	0.01	0.08	0.06	0.07	0.05	0.12	0.01
□ (M1)	0.95	0.96	0.95	0.96	0.84	0.91	0.87	0.90	0.82	0.97
Mg (M2+M3)	0.08	0.29	0.10	0.16	0.07	0.03	0.24	0.22	0.08	0.19

Fe^{2+} (M2+M3)	0.05	0.18	0.08	0.10	0.07	0.07	0.28	0.21	0.17	0.22
K	0.62	0.45	0.60	0.75	0.70	0.40	0.84	0.90	0.70	0.99
Na	0.04	0.03	0.03	0.00	0.00	0.05	0.00	0.00	0.00	0.03
Ca	0.00	0.06	0.00	0.00	0.00	0.02	0.00	0.00	0.00	0.00
v	0.35	0.46	0.37	0.25	0.30	0.53	0.16	0.10	0.30	0.00

902

903 Table 2: Selection of TEM-EDX analyses of Gulf Coast chlorites: crystal rim analyses with
904 the highest ^{IV}Al content for each *P-T*. Atomic contents are given in atoms per formula unit
905 (O=14 apfu), and M1, M2, M3 and M4 represent the cationic sites as defined by Vidal et al.
906 (2005, 2006). All iron is considered as ferrous, value in bold indicates an analysis excluded by
907 Vidal's model (Si > 3 apfu).

908

Sample	AZ#159 9230	ST#470 10717	CK#2 11924	CK#2 12196	LA#1 13559	ST#356 14501	CW#1 14277	WR#C1 17805	FR#1 18946	AL#1 19110	AL#1 20711
Analysis	chl28	chl30	chl50	chl20	chl23	chl34	chl31	chl16	chl29	chl25	chl29
BHT (°C)	102	121	129	135	149	166	191	191	204	216	232
BHP (bars)	300	590	660	690	850	800	750	1050	1150	1150	1200
Si	2.91	**3.01**	2.90	2.96	2.88	2.71	2.63	2.90	2.84	2.61	2.85
Ti	0.00	0.01	0.01	0.00	0.00	0.00	0.01	0.00	0.01	0.00	0.00
^{IV}Al	1.09	0.98	1.09	1.03	1.12	1.28	1.37	1.10	1.15	1.38	1.15
^{VI}Al	1.77	1.79	1.89	1.82	1.79	1.71	1.84	1.85	1.50	1.78	1.48
ΣAl	2.86	2.77	2.98	2.85	2.91	3.00	3.21	2.95	2.64	3.16	2.64
ΣFe^{2+}	2.46	2.53	2.37	2.45	3.28	2.07	3.01	2.48	2.15	2.44	2.93
ΣMg	1.39	1.22	1.31	1.34	0.53	1.98	0.85	1.28	2.11	1.55	1.36
Mg (M1)	0.22	-	0.19	0.20	0.08	0.26	0.09	0.18	0.36	0.17	0.23
Fe^{2+} (M1)	0.39	-	0.35	0.37	0.52	0.27	0.32	0.36	0.37	0.27	0.51
Al (M1)	0.09	-	0.09	0.03	0.12	0.28	0.37	0.10	0.15	0.38	0.15
□ (M1)	0.29	-	0.37	0.39	0.27	0.19	0.22	0.36	0.12	0.17	0.11
Mg (M2+M3)	1.17	-	1.12	1.14	0.44	1.72	0.76	1.09	1.75	1.38	1.12
Fe^{2+} (M2+M3)	2.07	-	2.03	2.08	2.76	1.80	2.69	2.12	1.78	2.17	2.43
Al (M2+M3)	0.67	-	0.79	0.78	0.66	0.43	0.48	0.75	0.35	0.40	0.33
Al (M4)	1.00	-	1.00	1.00	1.00	1.00	1.00	1.00	1.00	1.00	1.00
XFe^{3+}	0.28	0	0.23	0.28	0.20	0.05	0.05	0.22	0.36	0.05	0.27

909

910 Table 3: Clay thermometry models tested in this study.

911

Model	Type	Variables	Assumptions	Other components
Chlorite models				
Cathelineau and Nieva (1985)	Empirical	*T*	^{IV}Al increase with *T*	

Walshe (1986) (1)	Thermodynamic	*T*	Chl+qz equilibrium	Random cation mixing
Kranidiotis and McLean (1987)	Empirical	*T*	^{IV}Al increase with *T*	Correction of bulk composition effect from Fe/(Fe+Mg)
Cathelineau (1988)	Empirical	*T*	^{IV}Al increase with *T*	
Jowett (1991)	Empirical	*T*	^{IV}Al increase with *T*	Correction of bulk composition effect from Fe/(Fe+Mg)
Hillier and Velde (1991)	Empirical	*T*	^{IV}Al increase with *T*	
Zang and Fyfe (1995)	Empirical	*T*	^{IV}Al increase with *T*	Correction of bulk composition effect from Fe/(Fe+Mg)
Xie et al. (1997)	Empirical	*T*	^{IV}Al increase with *T*	Correction of bulk composition effect from Fe/(Fe+Mg)
Vidal et al. (2006)	Thermodynamic	*T-P*	Chl+qz including non-ideality	Ordered cation mixing
Inoue et al. (2009)	Thermodynamic	*T*	Chl+qz	Random cation mixing Semi-empirical equation
Illite/mica-like models				
Battaglia (2004)	Empirical	*T*	K increase with *T*	Correction of bulk composition effect from |Fe-Mg|
Dubacq et al. (2010)	Thermodynamic	*T-P* hydration	Mica-like+qz including non-ideality	Ordered cation mixing
Illite+chlorite models				
Walshe (1986) (2)	Thermodynamic	*T*	Chl+mica+qz+feldspar	Random cation mixing
Vidal et al. (2006) + Dubacq et al. (2010)	Thermodynamic	*T-P*	Multi-equilibirum	Ordered cation mixing

912

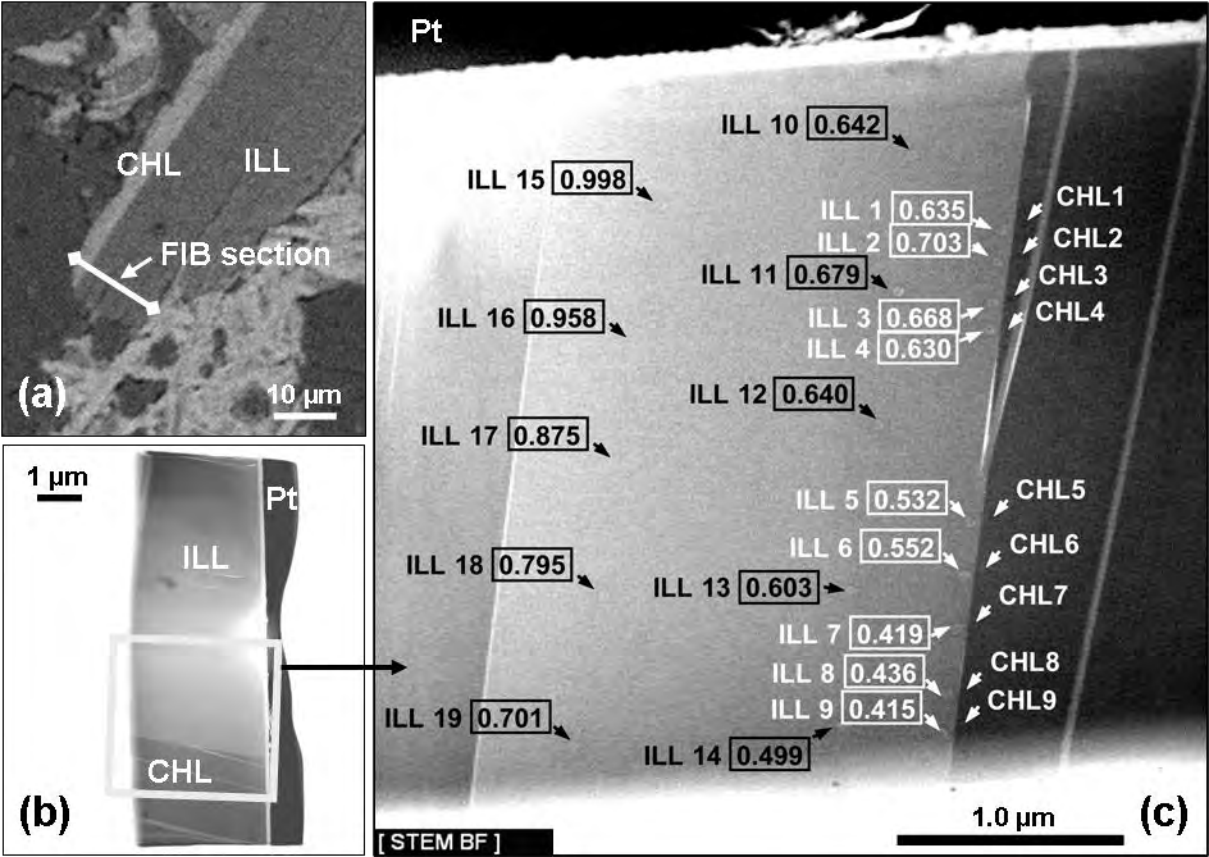
CHL
ILL
FIB section
(a)
10 µm
1 µm
Pt
ILL
CHL
(b)
Pt
ILL 10 0.642
ILL 15 0.998
ILL 1 0.635
ILL 2 0.703
ILL 11 0.679
ILL 16 0.958
ILL 3 0.668
ILL 4 0.630
ILL 12 0.640
ILL 17 0.875
ILL 5 0.532
ILL 6 0.552
ILL 18 0.795
ILL 13 0.603
ILL 7 0.419
ILL 8 0.436
ILL 9 0.415
ILL 19 0.701
ILL 14 0.499
CHL1
CHL2
CHL3
CHL4
CHL5
CHL6
CHL7
CHL8
CHL9
[STEM BF]
1.0 µm
(c)

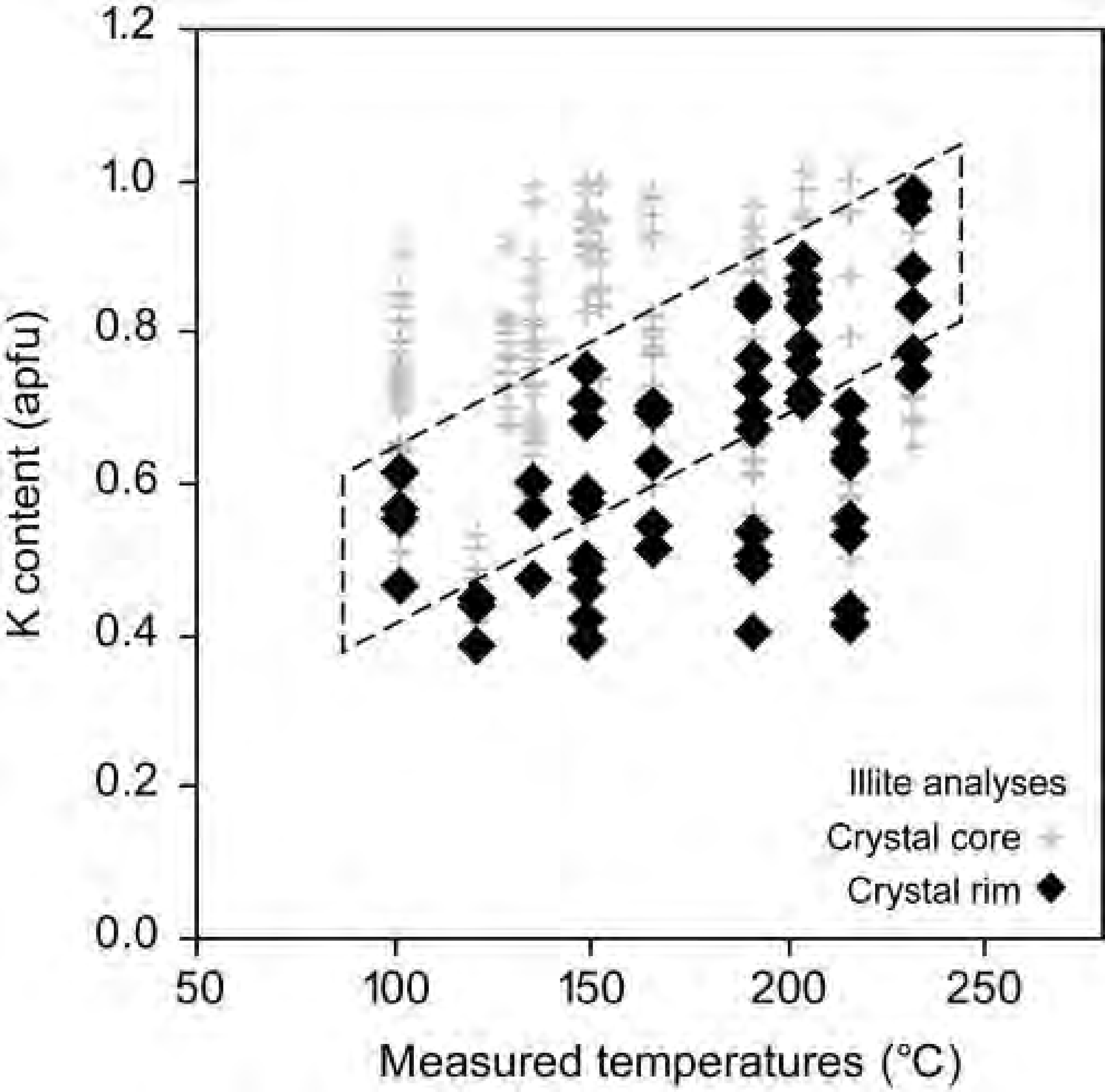
1.2
1.0
0.8
0.6
0.4
0.2
0.0
K content (apfu)
50
100
150
200
250
Measured temperatures (°C)
Illite analyses
Crystal core
Crystal rim

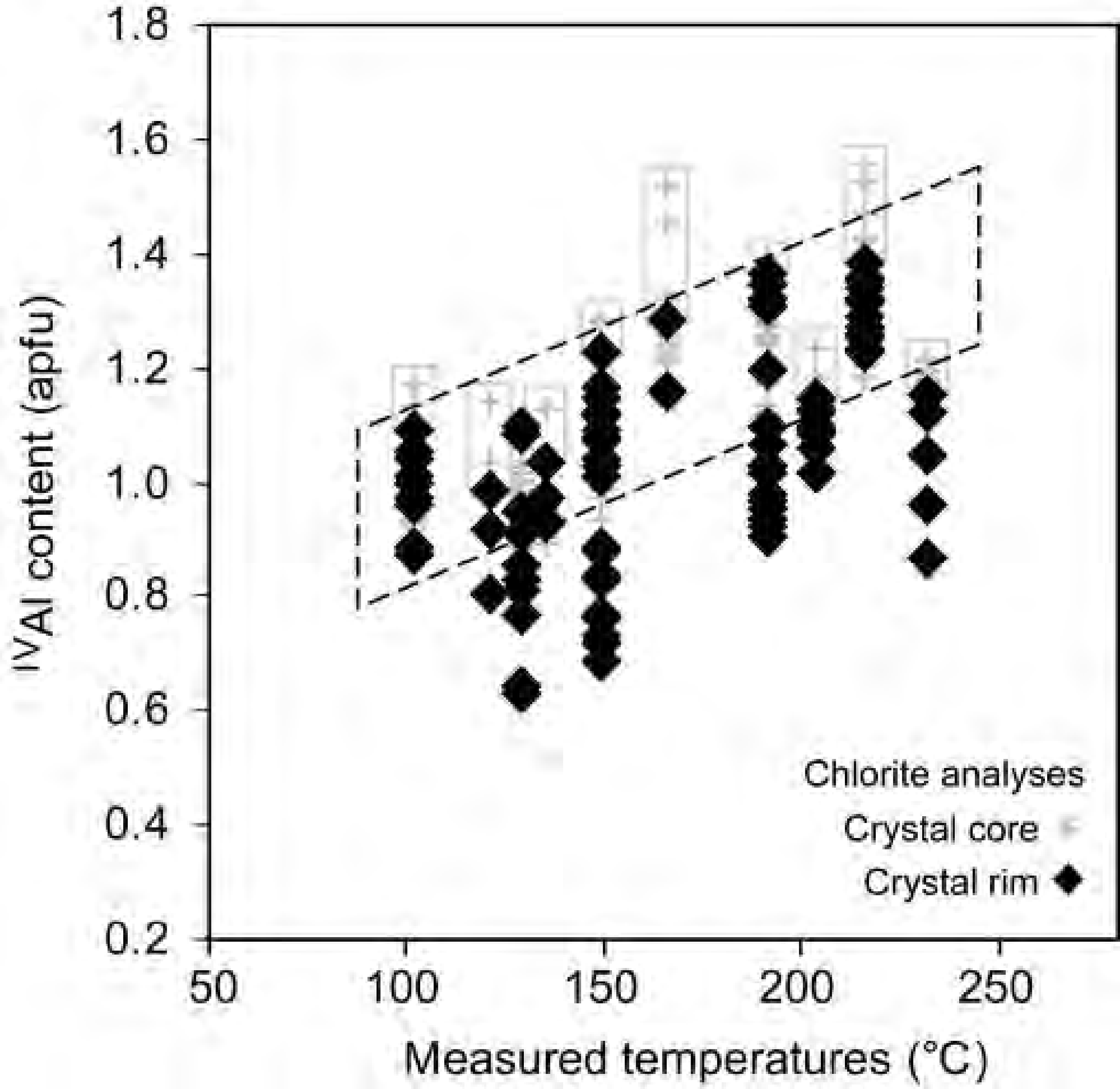
1.8
1.6
1.4
1.2
1.0
0.8
0.6
0.4
0.2
IVAl content (apfu)
50
100
150
200
250
Measured temperatures (°C)
Chlorite analyses
Crystal core
Crystal rim

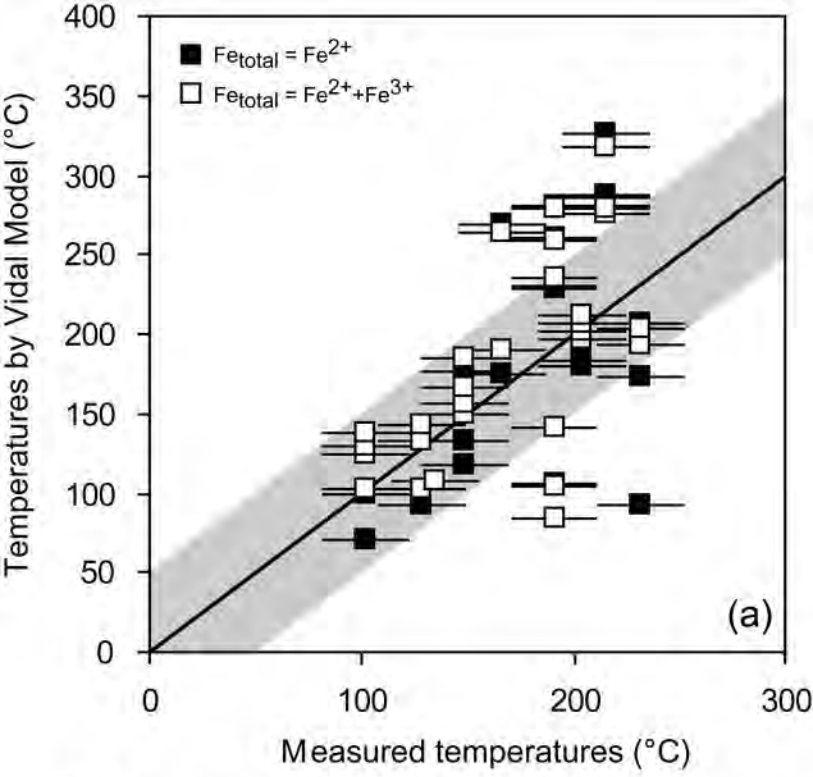
Fe$_{total}$ = Fe^{2+}
Fe$_{total}$ = Fe^{2+}+Fe^{3+}
Temperatures by Vidal Model (°C)
Measured temperatures (°C)
(a)
0
50
100
150
200
250
300
350
400
0
100
200
300

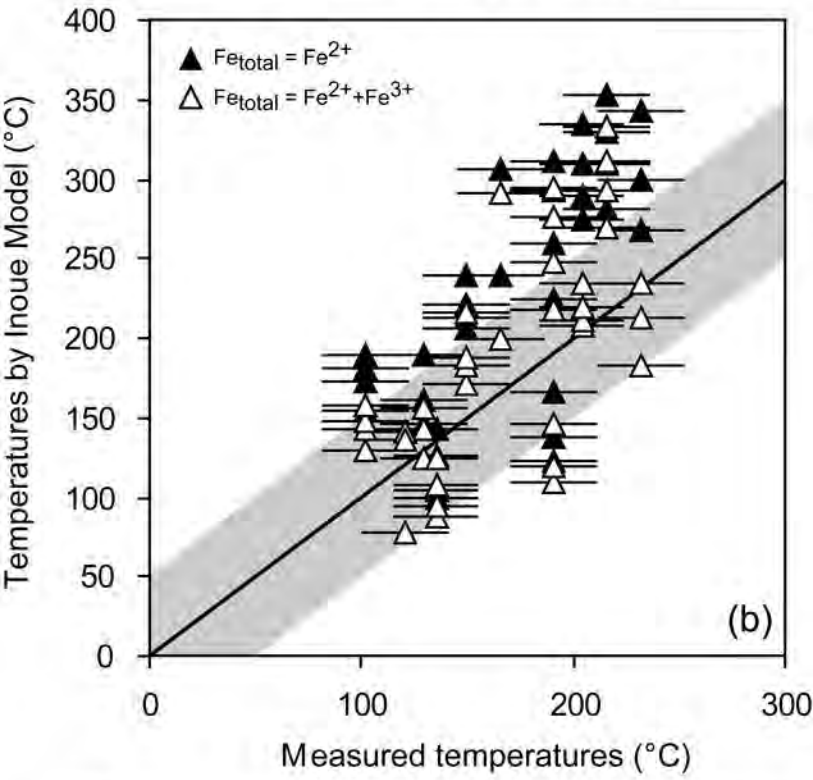
Fe$_{total}$ = Fe^{2+}
Fe$_{total}$ = Fe^{2+}+Fe^{3+}
Temperatures by Inoue Model (°C)
Measured temperatures (°C)
(b)
0
50
100
150
200
250
300
350
400
0
100
200
300

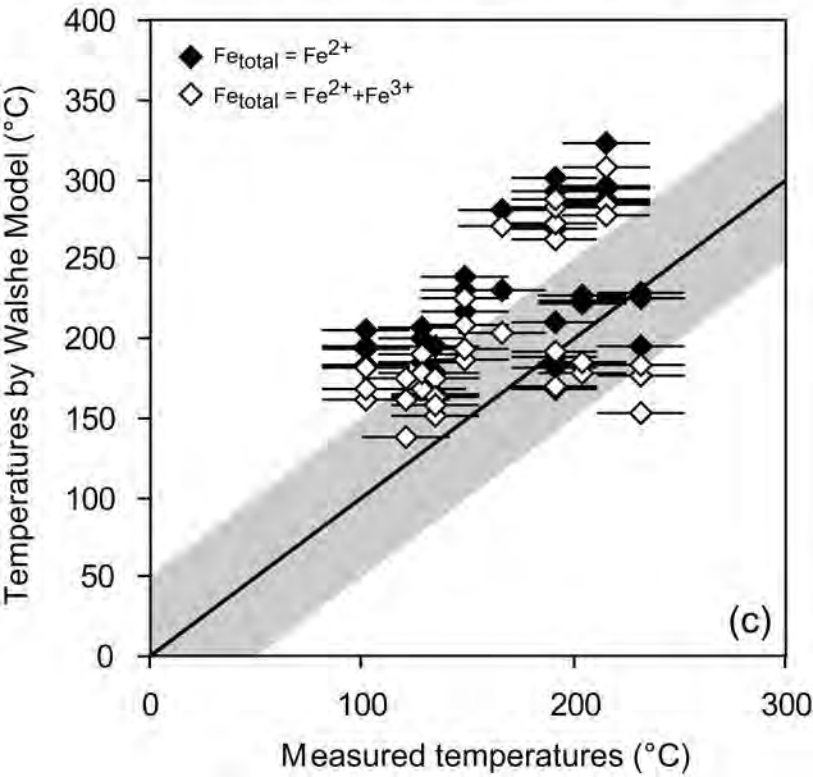
Fe$_{total}$ = Fe^{2+}
Fe$_{total}$ = Fe^{2+}+Fe^{3+}
Temperatures by Walshe Model (°C)
Measured temperatures (°C)
(c)
0
50
100
150
200
250
300
350
400
0
100
200
300

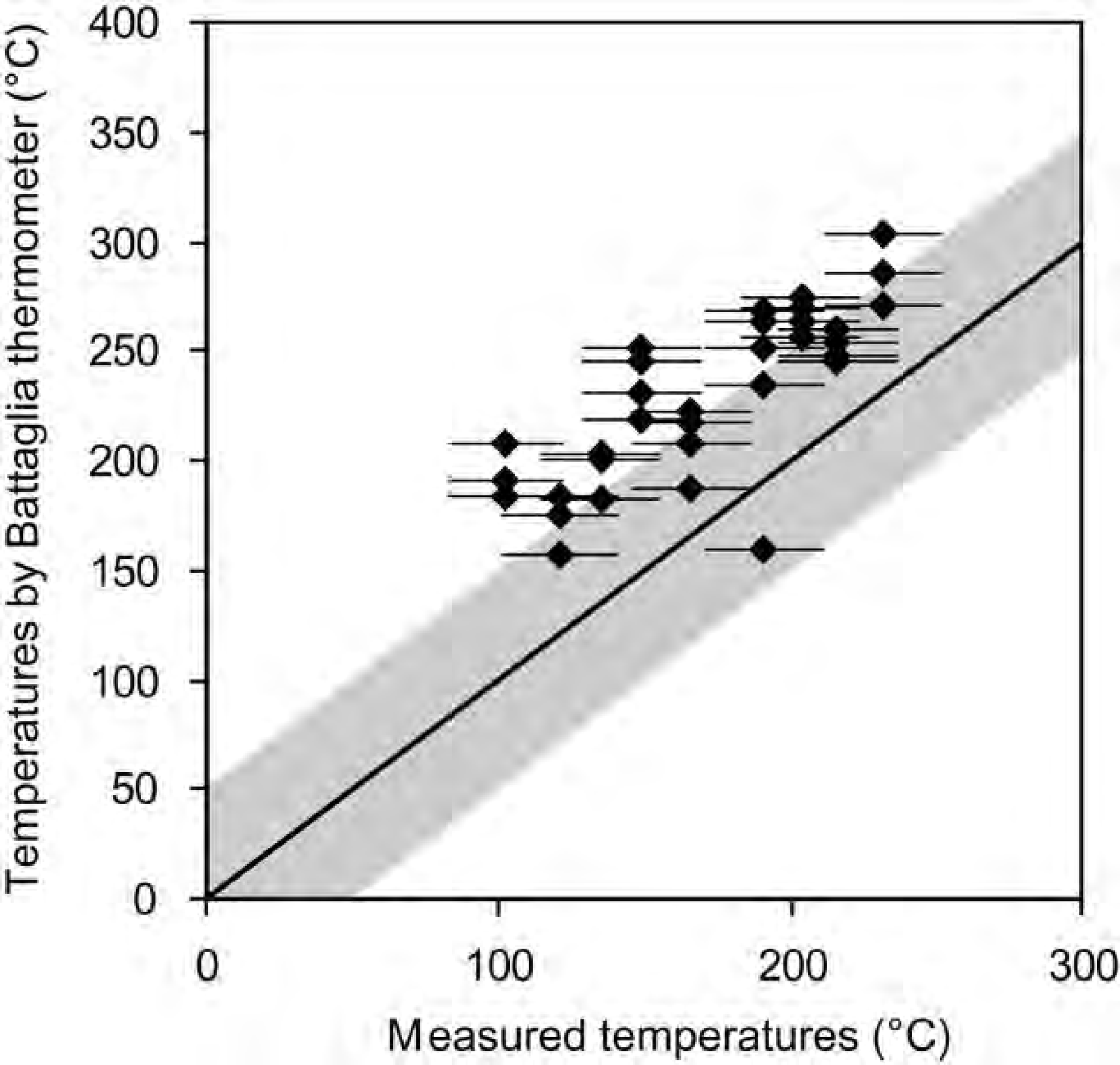
Temperatures by Battaglia thermometer (°C)
400
350
300
250
200
150
100
50
0
0
100
200
300
Measured temperatures (°C)

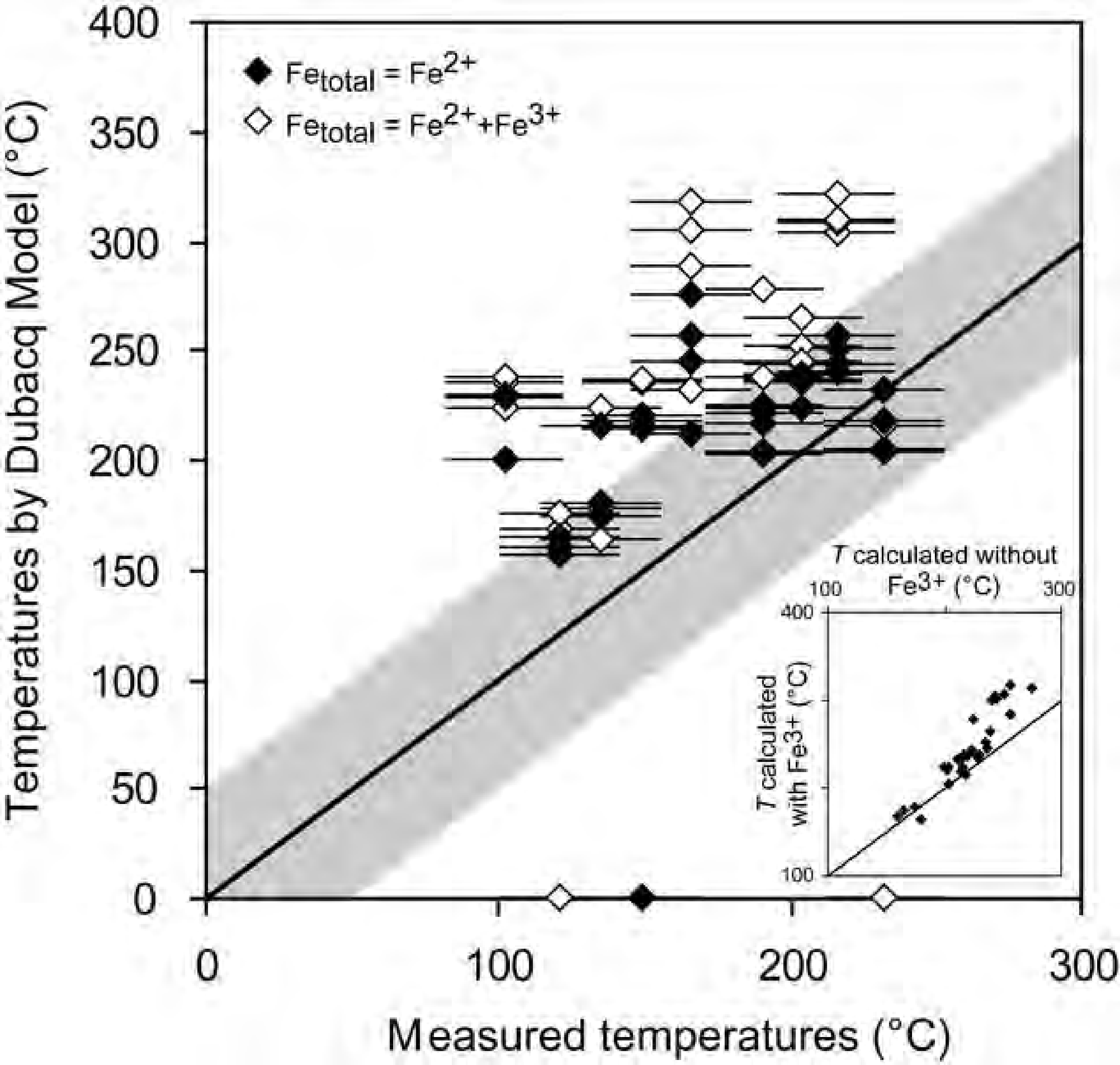
Fe$_{total}$ = Fe^{2+}
Fe$_{total}$ = Fe^{2+}+Fe^{3+}
Temperatures by Dubacq Model (°C)
Measured temperatures (°C)
0
50
100
150
200
250
300
350
400
0
100
200
300
T calculated without Fe3+ (°C)
T calculated with Fe3+ (°C)
100
300
400
100

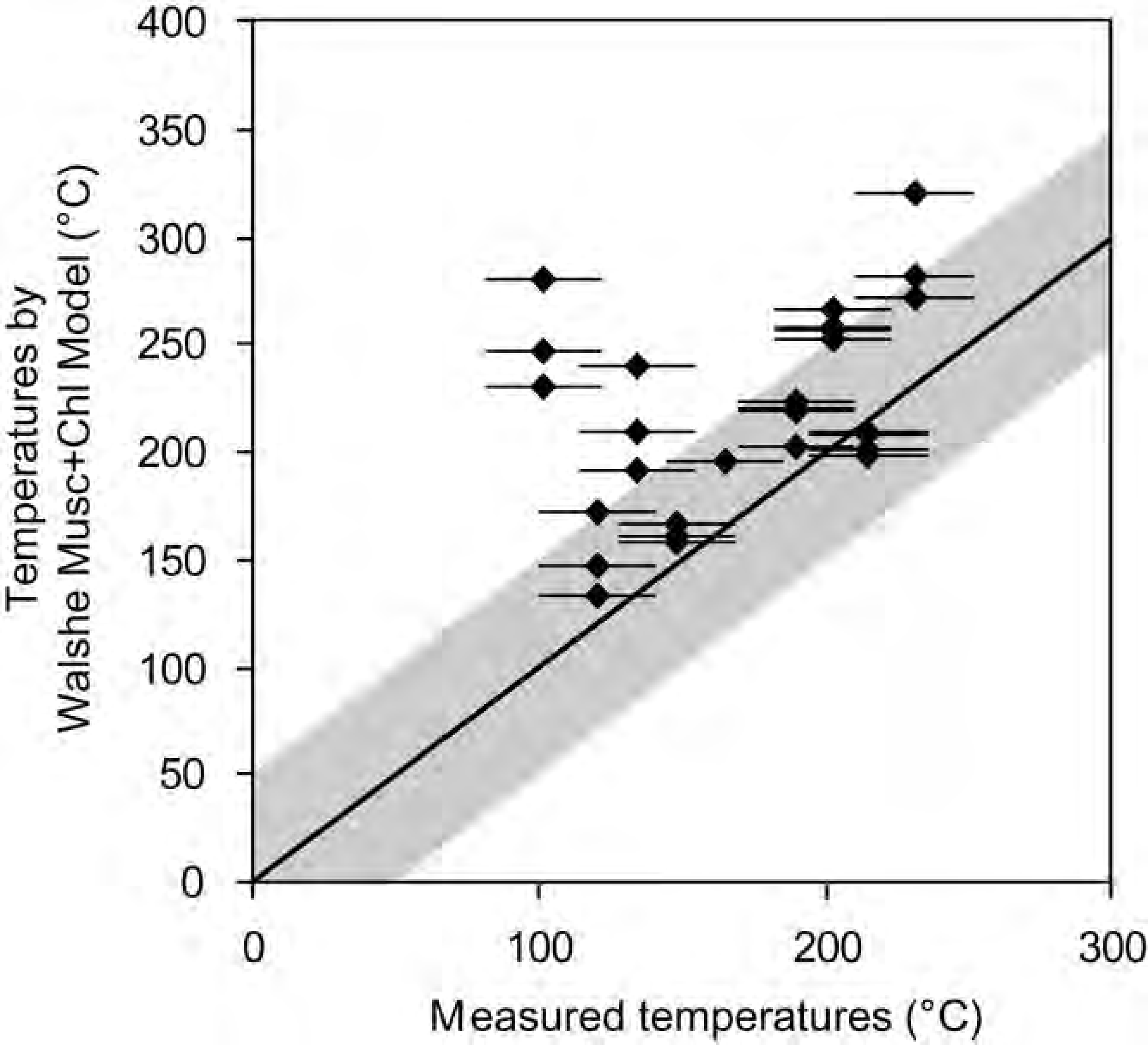
Temperatures by
Walshe Musc+Chl Model (°C)
400
350
300
250
200
150
100
50
0
0
100
200
300
Measured temperatures (°C)

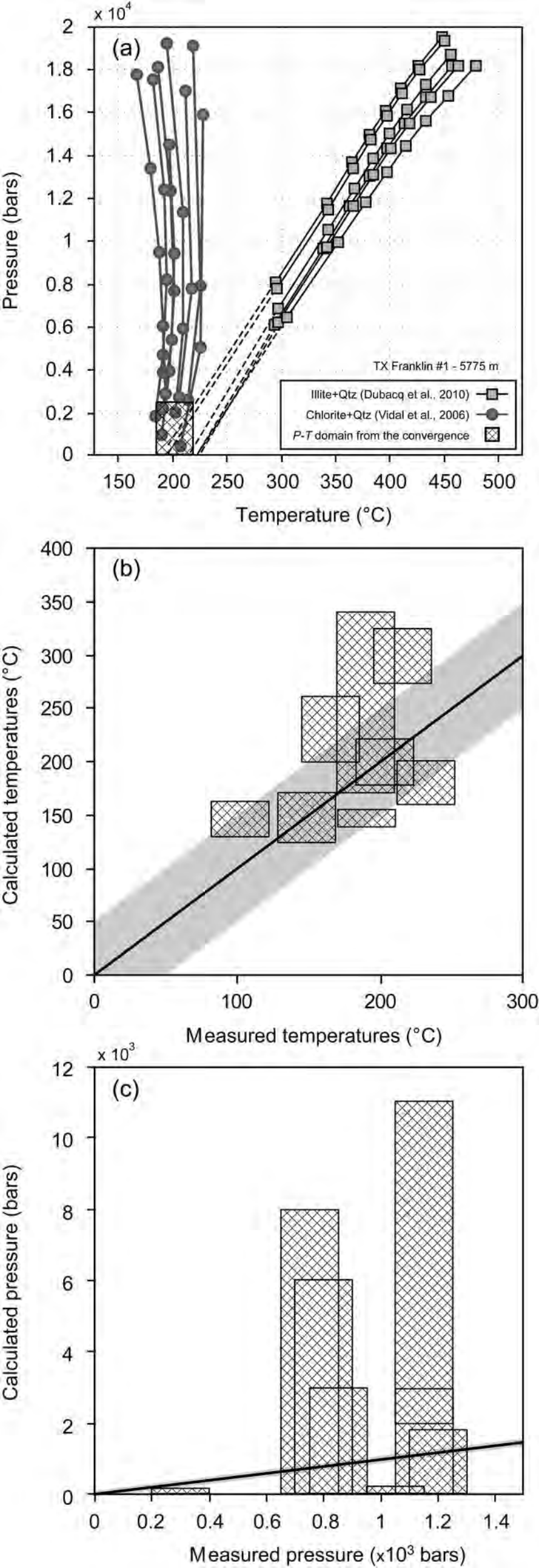
(a)
x 10^4
Pressure (bars)
Temperature (°C)
TX Franklin #1 - 5775 m
Illite+Qtz (Dubacq et al., 2010)
Chlorite+Qtz (Vidal et al., 2006)
P-T domain from the convergence
(b)
Calculated temperatures (°C)
Measured temperatures (°C)
(c)
x 10^3
Calculated pressure (bars)
Measured pressure (x10^3 bars)

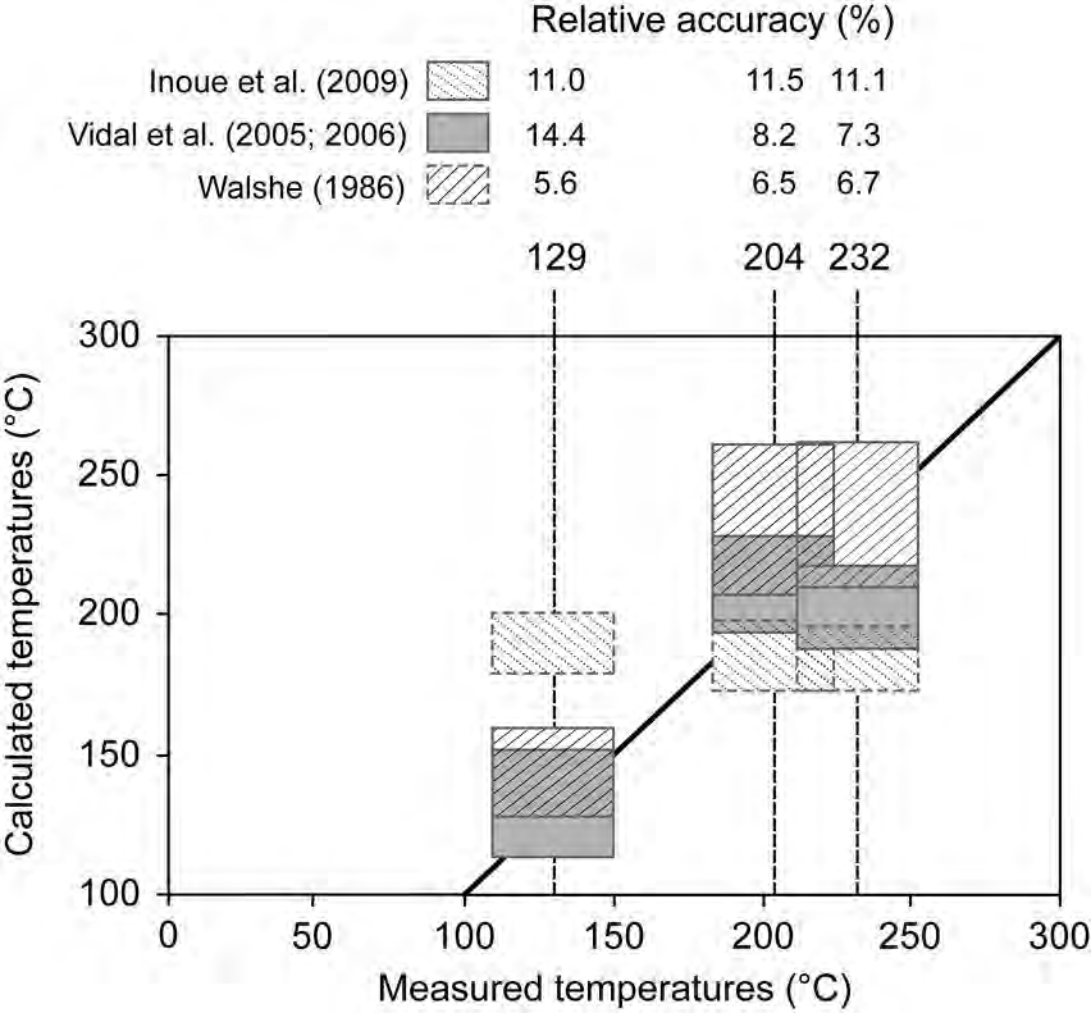
Relative accuracy (%)
Inoue et al. (2009)
11.0
11.5
11.1
Vidal et al. (2005; 2006)
14.4
8.2
7.3
Walshe (1986)
5.6
6.5
6.7
129
204
232
300
250
200
150
100
Calculated temperatures (°C)
0
50
100
150
200
250
300
Measured temperatures (°C)